Monte-Carlo-Simulation eines Ionenproduktionsringes für eine Beta-Beam Neutrinoanlage

von

Jakob Wehner

Bachelorarbeit in Physik

vorgelegt der
Fakultät für Mathematik, Informatik und Naturwissenschaften
der RWTH Aachen

im September 2009

angefertigt im
III. Physikalisches Institut B

bei

Prof. Dr. Achim Stahl

Monte Carlo simulation of an ion production ring for a beta beam neutrino facility

Bachelor thesis

Jakob Wehner

RWTH Aachen University
Supervisor: Prof. Dr. Achim Stahl

CERN - Conseil Européen pour la Recherche Nucléaire
Co-Supervisor: Dr. Elena Wildner

Abstract:

C. Rubbia et al. present in [1] a proposal for the production of radioactive isotopes ($^{8}_{3}$Li and $^{8}_{5}$B) which can be used to produce a Beta Beam to study neutrino oscillation physics. Low-energy Lithium ions ($^{7}_{3}$Li or $^{6}_{3}$Li) with $\beta_r \approx 0.1$ traverse a thin supersonic gas jet target ($^{2}_{1}$H or $^{3}_{2}$He). The outgoing produced ions have a favourable angular and energy distribution and leave a thin target, which makes a trapping of the produced ions improbable. Thus an efficient collection could be possible. Along with the energy deposition into the target a cooling technique, called "ionization cooling", needs to be studied. As D. Neuffer, [2], pointed out, beam cooling in all directions is not possible without introducing special coupling techniques to compensate heating effects. As part of this thesis, a first exploration of hadronic inelastic models, which are implemented in the well-known simulation software Geant4 and are used to describe the ion production, is done. Properties of the gas target, needed to introduce longitudinal cooling, are studied and a simple tracking code is implemented around a Geant4 simulation program to study the particle behaviour in a production ring lattice, described by M. Schaumann, [3].

Acknowledgement

First of all I would like to thank Prof. Achim Stahl and Elena Wilder for the opportunity to write the thesis at CERN. The financial support, provided by the following contracts, makes the stay at CERN possible. Thanks!

- FP6 "Structuring the European Research Area" programme, "CARE", contract number RII3-CT-2003-506395
- FP7 "Capacities Specific Programme, Research infrastructures", "EUROnu", Grant agreement number 212372

I would like to thank Prof. Achim Stahl for bringing this thesis a little bit to shape without getting tired. Thank you very much!

I would like to thank Elena Wildner, Elena Benedetto, Christian Hansen, Simone Gilardoni for the support at CERN and Gunter Folger for the help with the Geant4 models and the possibility to talk about Geant4 and the results of the simulations.

I would like to express my thanks to Bernhard Holzer and Werner Herr for the interesting, helpful and instructive discussions about accelerator physics and other funny topics.

Last but not least I would like to thank Sonja Urbahn and my parents, not directly involved in the creation of the thesis, for the mental support during the stay at CERN.

Many thanks to all of you!

Contents

1 Introduction

1.1 Beta beams

With the discovery of the solar neutrino deficit by Raymond Davis's Homestake experiment a new field of physics, called neutrino oscillation, was founded. Thanks to the difference between the neutrino flavour and mass eigenstates, one flavour eigenstate is a linear combination of all mass eigenstates:

$$|\nu_\alpha >= \sum_i U^*_{\alpha,i} \cdot |\nu_i > \qquad \text{where} \quad \alpha = e, \mu, \tau \quad \text{and} \quad i = 1, 2, 3 \tag{1.1}$$

$U_{\alpha,i}$ is the Maki–Nakagawa–Sakata or neutrino mixing matrix which describes the mixture between the flavour and mass eigenstates. The matrix can be expressed with a special parametrisation containing three mixing angles and one phase factor δ_{CP}. The mixing angles θ_{12}, θ_{13} and θ_{23} describe the mass mixture of the neutrino flavours and δ_{CP} the strength of the CP violation. Due to this mixture of mass and flavour eigenstates, a propagating neutrino, starting for instance as electron neutrino, can be measured later-on as a μ neutrino. The probability to measure a certain flavour eigenstate is oscillating during the propagation. This leads to the name Neutrino oscillation. While θ_{12} and θ_{23} are experimentally determined, there exists only an upper limit for θ_{13}. δ_{CP} is unknown. These two values need to be measured in the future.

Therefore a neutrino source or beam is needed which can be directed onto a neutrino detector, for example a Water Cerenkov detector like Super-Kamiokande. There exists an idea or method to create such a neutrino beam called "Beta Beams": Radioactive isotopes are accelerated and stored in a decay ring where the isotopes do a β^+ or β^- decay. Thus an electron neutrino or antineutrino is produced. These neutrinos are due to the Lorentz boost collimated to a beam which can be directed onto the neutrino detector which is usually located several hundreds of kilometres away. Not every isotope, doing a β decay, can be used to build a beta beam. The life time of the isotope needs to be reasonable short, around one second. Two pairs of β^+ and β^- emitter are discussed:

$$^8_5\mathrm{B} \rightarrow ^8_4\mathrm{Be} + e^+ + \nu_e \quad \text{and} \quad ^8_3\mathrm{Li} \rightarrow ^8_4\mathrm{Be} + e^- + \bar{\nu}_e \tag{1.2}$$

$$^{18}_{10}\mathrm{Ne} \rightarrow ^{18}_9\mathrm{F} + e^+ + \nu_e \quad \text{and} \quad ^6_2\mathrm{He} \rightarrow ^6_3\mathrm{Li} + e^- + \bar{\nu}_e \tag{1.3}$$

These ions have to be produced in an efficient way to make a Beta Beam possible. This thesis is focused on the production of $^8_3$Li and $^8_5$B.

Carlo Rubbia et al. present in [1] an idea for a production ring where a Li-7 beam (for the Li-8 production) or a Li-6 beam (for the B-8 production) is circulation in a storage ring traversing each turn a deuterium or He-3 target to produce the desired ions. Thanks to this permanent production and an efficient capture method the number of useful ions, decaying in a straight section in the decay ring to build the neutrino beam, could be large enough to reach a sufficient high beam intensity and therefore an adequate detection rate in the neutrino detector.

1.2 Accelerator physics

A particle travels in the production ring along the lattice elements (quadrupole, dipoles etc.). The reference or design orbit describes the path an ideal particle, which fulfils exactly the design conditions,

will take around the ring. The particle's position on this orbit is s with a range of $[0, C[$, where C is the circumference of the ring. If the particle is not ideal, the particle's position will not be on the reference orbit. It will have some offset to the design orbit. To describe this offset a right-handed coordinate system (x, y, s) is fixed to the reference orbit and follows the ideal particle. The x axes points outwards from the ring and y orthogonally upwards. The horizontal plane is created by s and x, the vertical by s and y. By looking at a particle bunch, some particles will be faster, some slower. The difference in their energy ΔE is measured against the design energy E_0: $\Delta E = E - E_0$. The time delay Δt, with which for example a slower particle arrives at a certain point in a lattice compared to the synchronous particle (ideal particle), can be used to describe the position of a particle in reference to the synchronous one along the s axis. With x, y and Δt it is possible to describe the particle position in reference to the ideal particle.

The particle oscillates around the reference orbit. It has therefore not only an offset to the reference orbit. It has also a movement direction which is described through $x' = dx/ds$ and $y' = dy/ds$. The arcus tangens of these magnitudes describes the angle between s and the projected movement direction onto the horizontal or vertical plane. Due to the fact that these angles are very small and the argument of the tangens can be replaced by the argument itself, x' and y' are used in the following also for the name of the angles.

The transversal size of a particle beam is described with two variables: The emittance ϵ and the betatron function β. Assuming energy conservation for the particles, the position in the phase space of each particle at a certain point in the lattice will be on an ellipse. The exact position on the ellipse is depending on the tune Q. The tune is the number of oscillations a particle is doing around its reference orbit at each turn. Each particle has its own ellipse. The area of the ellipse, also called "Courant-Snyder invariant", will be conserved because of the energy conservation. It depends on the initial conditions. The size of the ellipse's area which contains 69% of the other ellipses is called emittance, which corresponds to one σ of a gaussian distribution. Without energy conservation, the "Courant-Snyder" invariant is non existing, but the definition of the emittance can be kept if the emittance is defined as the RMS of a two dimensional gaussian distribution in the phase space, if a gaussian distribution is assumed. Consequently there exists for each plane (longitudinal, horizontal, vertical) one emittance.

The shape of the ellipse in the phase space will change when the particle traverses magnetic elements. To describe the deformation, the betatron function is used. The one σ envelope $E(s)$ of the beam is given by:

$$E(s) = \sqrt{\beta(s) \cdot \epsilon} \tag{1.4}$$

If the particle has some momentum deviation $\Delta p/p$ from the design particle (particle with the design energy), the deflecting effect of magnetic elements will be different. Consequently the particle will not oscillate around the reference orbit anymore, it will follow another new closed orbit around the machine. The transversal displacement of the particle due to the separation of its closed orbit from the reference orbit is described with a magnitude called dispersion. The particle, measured against the reference orbit, will have the following additional displacement.

$$\Delta x = D_x \cdot \frac{\Delta p}{p} \tag{1.5}$$

$$\Delta y = D_y \cdot \frac{\Delta p}{p} \tag{1.6}$$

A more detailed description of these issues can be found in [4].

1.3 Ion production and reverse kinematics

The purpose of the production ring is to produce ions which can be used as a beta beam. In the case under consideration the production of Li-8, the anti-neutrino emitter, and B-8, the neutrino emitter, are studied. To produce the desired ions a beam of Li-7 or Li-6 is injected into a production ring. It circulates and crosses a target on every turn. The target needs to be of a specific material to make the production possible. The ions can be produced by the following reactions:

$$^{7}_{3}\mathrm{Li} + {}^{2}_{1}\mathrm{H} \rightarrow {}^{8}_{3}\mathrm{Li} + p \tag{1.7}$$

$$^{6}_{3}\mathrm{Li} + {}^{3}_{2}\mathrm{He} \rightarrow {}^{8}_{5}\mathrm{B} + n \tag{1.8}$$

It is also possible to use the lighter particles as the incident one and the heavier as targets. This is called the normal kinematic frame [1]. This frame has some disadvantages: The incident particles are much lighter than the target particles. The resulting angular distribution of the produced ions will be wide and the kinetic energy small. The probability that the produced particles will come to rest inside the target will be high. The circulating deuteron or He-3 beam will deposit energy into the target. The amount of energy will be large due to the high intensity of the beam which is needed to produce enough Li-8 or B-8 ions per second (approx. 1 MW [1]). To remove the energy a fast moving traget is needed, potentially a liquid target. To avoid problems with extraction from the liquid target reverse kinematics is preferred.

In the reverse kinematics Li-6 or Li-7 are used as projectiles, impacting on a He-3 or deuteron target. A kinetic energy of 25 MeV is proposed. This target will be a supersonic gas-jet. The thickness of the target should be small to avoid the trapping of the produced ions. The outgoing angular and energy distribution are narrower than in the normal kinematical frame and the kinetic energies are higher. The outgoing ions will form a narrow angular cone.

To collect the Li-8 and B-8 ions, a ring-formed device is needed. This device is located behind the target and has a hole in its center to allow the traversal of the circulating beam through the capture device without being caught. The ring has to cover the angular region of the produced ions to allow a great enough ion production per second. It is questionable if the angular distribution allow an efficient separation of the produced ions from the circulating ones. If most of the produced ions have a small production angle, an efficient collection with a ring device is not possible unless the hole of the device is so small that also circulating ions are caught. This will also destroy the circulating beam.

The ions will be stopped in the device with tantalum stoppers and are extracted as a neutral gas which can afterwards be ionized and accelerated into a decay ring. The techniques to provide such a device are used at ISOLDE.

As part of this thesis, Geant4 is used to simulate the production of the ions to study the angular and energy distribution of the generated ions. Therefore models, implemented in Geant4, have to be investigated and checked (see chapter 2).

1.4 Ionization cooling

In addition to the ion production the gas target has another very important purpose: it should provide conditions which makes a stable circulation of the beam possible. These conditions need to be studied to understand the requirements for the lattice and the target.

The processes, which have to be taken into account, were investigated in [1, 2]. Conditions for a stable run of the production ring are derived. A short introduction into the topic and the challenges is given in the following.

1.4.1 Transverse compression

When the particles in the bunch traverse the gas target, they get scattered which leads to an emittance growth. The emittance growth is estimated based on small changes in direction to:

$$\delta A_{scat} \approx \beta \cdot \overline{\delta x'^2}$$

Here A is the emittance, $\overline{\delta x'^2}$ is the mean squared projected scattering angle and β the value of the β-function at the target.

The energy loss of the particle has to be recovered. This is done with one or more cavities. A cavity adds momentum δp in the longitudinal direction, but not in transversal direction and changes therefore x' and y' accordingly to:

$$\delta x' = -x' \cdot \frac{\delta p}{p} \tag{1.9}$$

$$\delta y' = -y' \cdot \frac{\delta p}{p} \tag{1.10}$$

where x' and y' are the angles at the entrance of the cavity. From this angle reduction, a reduction of emittance is derived, [1]. After averaging over many turns the emittance is reduced by:

$$\frac{\overline{\delta A}}{A} = -\frac{\overline{U}}{2T} \tag{1.11}$$

Here $\overline{U}$ is the averaged energy loss in the target (positive) and T the average kinetic energy of the particles at the target. An energy loss of about 300 keV for a kinetic energy of 25 MeV is assumed [1]. This expression lead to an exponential decay of emittance A.

$$A(t) = A_0 \cdot \exp\left(-\alpha_{(x,y)} t\right) \tag{1.12}$$

$$\alpha_x = \alpha_y = f_s \cdot \frac{U}{2T} \tag{1.13}$$

where f_s is the revolution frequency of the ring. The two effects, namely the scattering emittance growth and the cavity induced reduction of the emittance, counterbalance each other and leads to an equilibrium emittance, [1]:

$$A_{eq} = 2T\beta \frac{\overline{\delta x'^2}}{\overline{U}} \tag{1.14}$$

1.4.2 Longitudinal cooling

The Li-7 or Li-6 ions have to traverse the gas target to produce the desired radioactive isotopes. This leads to a specific behaviour in the longitudinal motion. Compared to the energy loss effect in the gas target, synchrotron radiation provides damping in the longitudinal phase space ($\Delta E - \Delta\phi$ plane). The momentum dependence of the synchrotron ration which makes a faster particle loose more energy than a slower one leads to a damping effect. In our case the energy loss effect in the target is approximately described with the well-known Bethe-Bloch formula:

$$-\frac{dE}{dx} = K z^2 \frac{Z}{A} \frac{1}{\beta_r^2} \left[\frac{1}{2} \ln\left(\frac{2 m_e c^2 \beta_r^2 \gamma_r^2 T_{max}}{I^2} \right) - \beta_r^2 - \underbrace{\frac{\delta(\beta_r \gamma_r)}{2}}_{\approx 0 \text{ for small T}} \right] \tag{1.15}$$

where β_r and γ_r are the usual relativistic quantities. T_{max} is the maximum kinetic energy, which is transferable to a free electron in a single collision, and I the mean excitation energy (cf. [12]).

$$U = \int_0^d \underbrace{-\frac{dE}{dx} \cdot \rho}_{\approx \text{constant}} dx \approx -\frac{dE}{dx} \underbrace{\rho d}_{=:t_h} \tag{1.16}$$

U is the energy loss which can be approximately expressed with the Bethe-Bloch formula assuming dE/dx is nearly constant along the target thickness. The product of the target density ρ and the target thickness d is called thickness t_h. To get an energy loss of 300 keV for $T = 25$ MeV t_h has to be of the order of $300\,\mu g/cm^2$.

In the energy region, which is under consideration (25 MeV), a faster particle will loose more energy than a slower one. This leads to a phase disturbing effect (the too fast particle arrives at the wrong phase at the cavity). Therefore the longitudinal emittance is growing. The change of the particle's energy as a function of time is:

$$\Delta E(t) = A \exp(-\alpha_\epsilon t) \cos(\Omega_s t - B) \tag{1.17}$$

$$\alpha_\epsilon = \frac{f_s}{2} \cdot \frac{dU}{dE} \tag{1.18}$$

where Ω_s is the synchrotron frequency and where dU/dE is negative as already mentioned. Therefore the longitudinal emittance is growing. To compensate the effect the target is located in a dispersive area in the lattice. Assuming $D_x > 0$ and $D_y = 0$ at the point of the target, a too fast particle will arrive displaced with an increased x offset. If the target thickness d is growing for larger x the energy loss will also increase with x and thereby with E. A wedge shaped target could be used to increase dU/dE. If the angle at the tip of the wedge (the tip pointing to the centre of the ring), is great enough, dU/dE is swapping signs and longitudinal cooling can be obtained.

By looking at U as a function of x,

$$U \approx U_0 + \underbrace{\frac{dU}{dx}}_{=:U'} \underbrace{\delta x}_{=D_x \frac{\Delta p}{p}} = U_0 + \underbrace{U' D_x}_{=:V} \frac{\Delta p}{p} \tag{1.19}$$

it is obvious that V has to fulfil a certain condition. The cooling condition can be rewritten into:

$$\frac{dU}{dE} \rightarrow \left(\frac{dU}{dE}\right)_0 + \frac{1}{\delta E} \cdot U' D_x \cdot \underbrace{\frac{\Delta p}{p}}_{\delta E/2T} = \left(\frac{dU}{dE}\right)_0 + \frac{V}{2T} > 0 \tag{1.20}$$

$$\Rightarrow \quad V > -2T \left(\frac{dU}{dE}\right)_0 \tag{1.21}$$

where $(dU/dE)_0$ is the derivative of the energy loss with respect to particle energy without any wedge shape and dispersion assumptions.

1.4.3 Horizontal excitation

The fact that the target has to be located in a dispersive area leads to an additional effect in the horizontal motion. The closed orbits for different $\Delta p/p$ are due to the dispersion separated in the target region and the dispersion D_x is non-zero. By looking at one particle with a certain initial $\Delta p/p$ and zero displacement and a perfect direction, x' and y' are zero, the problem can be explained easily. A particle like this would follow exactly the closed orbit which belongs to the specific $\Delta p/p$. When the particle arrives at the gas wedge, it will loose energy. Therefore $\Delta p/p$ and also the closed orbit of the particle

changes. The position of the particle in physical space is however still the same by neglecting any small displacement due to the scattering in the target (a change in the direction is already considered above in section 1.4.1). Consequently the particle has now an x offset to its new closed orbit. When the particle traverses a dipole section, after which the dispersion is zero, the different closed orbits are joined together, but the displacement of the particle is kept. Therefore it is not an ideal particle for the specific $\Delta p/p$ anymore and a betatron oscillation is excited.

As a result, the damping has to be corrected.

$$\alpha_x = \frac{f_s}{2T}\left(U_0 - U' D_x\right) \tag{1.22}$$

Damping in the horizontal plane can only be obtained if α_x is larger than zero. Therefore the horizontal cooling condition is:

$$U_0 > U' D_x = V \tag{1.23}$$

1.4.4 A damping-heating problem and a possible solution

It is essential to obtain damping in both, the horizontal and the longitudinal, plane to increase the beam lifetime. By looking at both conditions a problem occurs:

$$U_0 \approx 0.3\,MeV \overset{1.23}{>} V \overset{1.21}{>} -2T\left(\frac{dU}{dE}\right)_0 \approx 0.5\,MeV \tag{1.24}$$

Both conditions can not be fulfilled at the same time. The sum of the damping rates α_x, α_y and α_ϵ is a constant, [2]. The damping rates in the different planes can be described using partition numbers. The concept of partition numbers is used for synchrotron radiation and are correspondingly defined as follows (cf. [4]):

$$\alpha_i = J_i \cdot \frac{f_s U}{2T} \tag{1.25}$$

As a result J_y is 1, $J_x = 1$ is for $U' = 0$ as well and J_ϵ can be derived to -1.6 for $U' = 0$, [2]. The sum of the partition numbers is constant and equal to 0.4. The idea to get damping into each plane is to introduce additional coupling between the different planes. This could in principle be possible because the sum of the partition numbers is positive. If the partition numbers could be changed to get for each plane for instance $J_i \approx 0.13$, the particle bunch will be cooled down in every dimension. Therefore longitudinal motion has to be mixed with the horizontal and vertical. Up to now only the horizontal and longitudinal motion are coupled due to the excitation effect of the target in the dispersive area.

As suggested in [2], a simple solenoid can be included into the lattice to exchange x and y phase space at each turn. The wedge formed target certifies that longitudinal cooling is obtained and the corresponding partition number should finally be $J_\epsilon \approx 0.13$. This increase in J_ϵ leads to a decrease in J_x. Without the coupling between x and y, J_x will turn so strong that it becomes negative and heating in this direction is introduced. By using the solenoid the decrease in partition number is counterbalanced on two partition numbers namely J_x and J_y. With the correct strength of the solenoid, calculated by [2], it should be possible to get for each plane a partition number of 0.13. Damping in each direction should consequently be possible.

As part of the thesis, Geant4 is used to study the condition for longitudinal cooling. In addition to that a tracking code is written which makes it possible to use the Geant4 target implementation to study the behaviour of particle in a production ring. The lattice, used for the study, is designed by [3].

1.5 Geant4

The software which is used in nearly all simulations of this thesis is Geant4. Geant4 is a toolkit written in C++ which provides all the tools needed for a simulation of the passage of particles through matter. The main application areas are high energy, nuclear, accelerator physics and the software can also be used in medical researches as well.

The simulation toolkit has to provide several things: tools to describe the geometry like a detector, to do tracking of a single particle through the geometry and also management tools to have control of runs, events and tracks. Geant4 is providing these things and contains moreover tools for visualization and user interaction.

The toolkit of Geant4 consists of a large amount of object oriented classes which allow the user to implement his own program to do a complex simulation. In fact only a few virtual classes need to be reimplemented by the user to write a simple simulation.

This reimplementation of virtual classes is one of the design ideas of Geant4. Thus the user is able to describe what he wants to describe (e.g. the detector geometry) without rewriting things not directly connected to the current design part. The reimplementation process takes place by inheriting from the predefined virtual classes of Geant4. These inherited classes, describing the experimental setup the user wants to describe, can be committed to the most central base class in Geant4: the so-called "Run Manager".

Due to this design concept Geant4 defines the superior structure of a simulation program but gives the user enough freedom to build many different simulation setups.

More and detailed information can be found on the website of the project
(http://geant4.cern.ch).

2 The ion production

As described in section 1.3 the reverse kinematical frame is used to produce the desired ions Li-8 or B-8. The heavier particles (Li-7 and Li-6) are used as projectiles. One would expect that the outgoing ions should have a small angular distribution (angle between the momentum directions of the incoming particle and the produced ion). A Geant4 simulation is presented here to study the kinematics of the ion production. As a first step, however, it has to be clarified if Geant4 contains models for the studied reaction in these low energy regions of about 25 MeV.

In the following the simulations are focused on the reaction Li-7(d,p)Li-8 because the expected cross section of this reaction is larger by a factor of ten than the one for the B-8 production. Fewer incoming events need to be simulated to produce a certain number of Li-8 events. Computing time is saved and a first test of the general validity of the model used could be done more efficiently. Nevertheless the validity has to be checked also for the B-8 production.

2.1 Preparations

2.1.1 The model problem

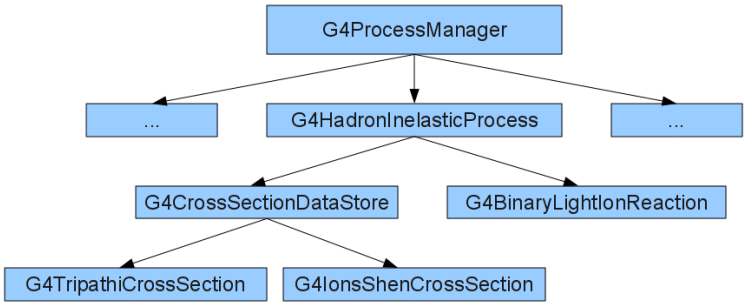

Figure 2.1: Sketch of the Geant4 process manager structure

Figure 2.1 shows a simple illustration of what Geant4 needs from the user. The "ProcessManager" contains information about the interaction possibilities for each particle. The user registers different processes with the process manager to include a certain interaction. In our case the particle should only interact through hadronic inelastic reactions. Therefore an object of the class "G4HadronInelasticProcess" is registered with the process manager. This object requires one model for the interaction and one for the inelastic cross section. In fact not only one model for the cross section can be applied. The user can apply any number of them with different validity ranges. Geant4 is able to switch between the different cross section models if one of them looses validity. The cross section model decides about the probability when the process starts to interact on the particle and the interaction model about the manner of the interaction (kinematics and also reaction cross section).

The incident particles are Lithium ions which are treated in Geant4 as so-called "generic ions". For this particle type there are only a handful of possible models for hadron inelatic interaction implemented in

Geant4. Each of these models has its own validity range concerning the kinetic energy of the incident particle. The simulated particles should have a kinetic energy of about 25 MeV which is below the lower energy limit of most or all of the models. There are only two models remaining for nucleus-nucleus interaction which have a small lower energy limit and should show reasonable results, [5]:

Binary light ion reaction model + Pre-compound model (in the following the name of the Geant4 class is used: G4BinaryLightIonReaction) is a modified version of the binary cascade model. The binary cascade model describes the inelastic interaction by simulating a binary interaction. This means that one nucleon of the incident particle or from a resulting secondary particle from a former interaction interacts with a nucleon of the target nucleus. The movement of the nucleon in the field of the nucleus is treated by a numerical integration of the equation of motion. The interaction cascade stops when the maximum and average kinetic energy of the secondaries fall below a threshold. For a system of light ions the initial state of the interaction consists of two nuclei where the lighter one is chosen as the incident particle. Its nucleons enter the cascade with certain momenta and positions. At the end of the cascade simulation the remaining target nucleus is treated by de-excitation models which are calculating the final equilibrium state of the particles, [6]. The lower end of the energy validity range is about 80 MeV. For low energies the nucleons of the incident nucleus and the target are accumulated into one nucleus whereby the excitation energy is chosen accordingly to the kinetic energies of the initial nuclei, [5]. For the resulting nucleus the pre-compound model is called to determine the final state of the nucleus by emitting protons, neutrons, deuterons, trithiums and helium nuclei (cf. [6]). With these modifications the Binary light ion reaction model can also treat technically energies below 80 MeV. The validity is questionable, [5].

QMD (quantum molecular dynamics) model (also called in the following G4QMD-Reaction) is a model where all nucleons in the participating nuclei are considered as gaussian wave functions in position and momentum. The peak of the gaussian distribution, namely the mean momentum and the mean position, develops accordingly to the Newtonian equations which are calculated using the Hamiltonian function. In principle this model is doing the same thing like the G4BinaryLightIonReaction model namely simulating the propagation of the nucleons through the target nucleus. In addition to the G4BinaryLightIonReaction model further improvements like Pauli principle, participant-participant scattering are introduced. The first version of the model was implemented in Geant4 version 9.1, so some features described in papers might not be included. Further information about the model itself can be found at [7]. The validity range extends down to 50 MeV.

The validity range is not a fixed limit. At these energies one has to expect that both models loose more and more accuracy. Both models are used as black boxes and results are compared. Theoretically study of this model is beyond the scope of this thesis.

There are five different cross section models for ions which can be applied to the G4Hadron-InelasticProcess. Each of these models has its own validity range for energy, [6]:

Shiver formula is an energy independent formula valid above 100 MeV per nucleon, [6].

Kox and Shen formula are based on the strong absorption model and are valid also for small energies. Below 30 MeV per nucleon the two models start to differ. At these regions the Shen formula should be used, [6]

Tripathi formula has a similar form as the Shen formula and can be used at energies below 1 GeV/N, [6]

Tripathi for "light systems" is a modification of the Tripathi formula especially for light system which are in this case deuteron, trithium, He-3 and alpha particles (cf. [6]).

The models containing the Shen and the Tripathi formula are used for the simulation because of the low kinetic energy which should be treated in the following.

For the G4BinaryLightIonReaction model a prepared physics list, containing information about the interaction possibilities of the particles, is used accordingly to the advice of [5]. There is however no prepared physics list for the QMD model, so a new one has been written and is used for the simulations.

2.1.2 Modelling the gas jet target

A detector needs to be designed. In our case a deuterium gas jet target is needed. There is no possibility in Geant4 to describe a supersonic gas jet. In [1] a jet velocity of about 2200 $\frac{m}{s}$ is discussed. The incident particles with a kinetic energy of 25 MeV and a mass of 6533.83 MeV/c^2 have by contrast a velocity of about $\beta_r c \approx 2.62 \cdot 10^7 \frac{m}{s}$. Neglecting the velocity of the gas particles should be a good approximation.

The geometry of the target is quite simple: a box-shaped target is placed in the center of the world volume which has to contain all target and detector parts (cf. [8]). The box has a thicknes d of 5 cm. The density of the gas jet is set to $0.0576 \frac{mg}{cm^3}$ which corresponds to an energy loss of around 300 keV for a 25 MeV particle. This value will be used later on in chapter 3.3. Special assumptions on the target geometry, like the wedge shape, are not made and will be introduced when the longitudinal cooling is studied. A special shaped target is not necessary to calculate cross sections and to determine the kinematics.

2.2 Cross sections

To check, if the models and physics lists used show a good performance, the reaction cross section, the models are delivering for the reaction Li-7(d,p)Li-8, is examined. In addition to that, also the total inelastic cross sections are calculated and compared to ensure that both physics list, containing the reaction models, are using the same inelastic cross section models.

2.2.1 Reaction cross section

Because the validity range of the models ends above the desired energies of about 25 MeV, the simulations start with a kinetic energy of about 100 MeV in the validity range. The kinetic energy is decreased step by step to the desired energy. Through this procedures anomalies of the models will become visible.

To calculate the cross section 10^9 incoming Li-7 particles are simulated. The Li-7 ions traverse the deuterium gas target and interact with a certain probability hadronically. If Li-8 is produced the event is saved in a output file. The 10^9 incoming events are separated into 20 jobs with 50 million each. For each of these jobs the seeds for the random number generator in the Geant4 program are initialized from the random number generator of the operating system (using the $random variable of the linux environment). The 20 jobs are statistically independent.

For each of these jobs the number of incoming events N_{tot} is known and also the number of the produced Li-8 ions N_{Li-8}. The interaction probability is estimated from $p = N_{Li-8}/N_{tot}$. This probability can also be expressed as a function of the reaction cross section σ_r, the number of target particles N_T and the illuminated front area of the target box A, [9]:

$$p = \frac{N_{Li-8}}{N_{tot}} = \frac{N_T \cdot \sigma_r}{A} \tag{2.1}$$

By using the illuminated volume of the target $V = A \cdot d$, where d is the thickness of the box in the direction of motion. The cross section is then:

$$\sigma_r = \frac{m_T}{\rho \cdot d} \cdot \frac{N_{Li-8}}{N_{tot}} \tag{2.2}$$

where m_T is the mass of a target particle and ρ the density of the target. In our case m_T is not the mass of a deuteron particle, it is, because of the chemical binding of two deuterons to a gas molecule (D-D), twice the mass of a deuteron.

20 values of the cross section are calculated for each incoming particle energy. The mean value and its error are calculated. The reaction cross section is plotted as a function of the incident particle energy in figure 2.2. The red points show the results from a measurement of deuteron scattering on Li-7 [10]. These results are for the normal kinematics frame and to get the reverse kinematical frame the energy scale has be changed by a linear transformation, [1]:

$$T_{Li} = 3.483 \cdot T_D \tag{2.3}$$

where T_{Li} is the kinetic energy for the Li-7 and T_D the kinetic energy for a deuteron beam.

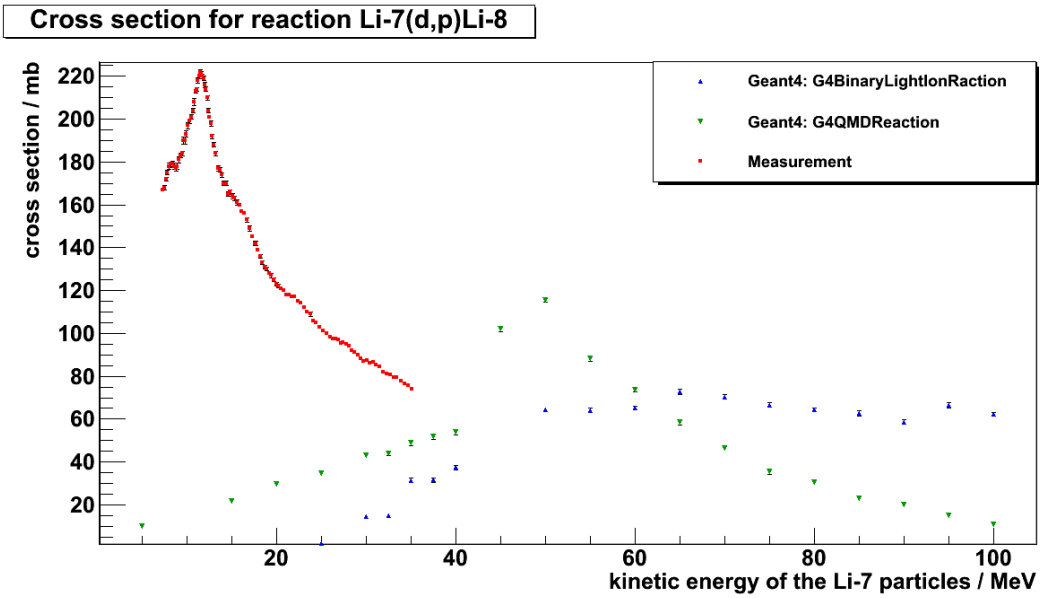

Figure 2.2: Reaction cross section as a function of the kinetic energy (red: measurement; blue: G4BinaryLightIonReaction; red: G4QMDReaction)

The green points show the result of the simulation with the G4QMDReaction model. The model shows a peak for the reaction cross section. Compared to the measurements the peak appears at a to high energy. In the region where measurements are available the results are completely different. Even the tendencies are wrong. The model shows no agreement with the measurement. Possibly the model could be optimized for the simulation to reproduce the measurements, [5].

The results for the G4BinaryLightIonReaction model can be seen in the blue points. They show a completely different behaviour. There is no peak and even at the upper energy end of the measurements the value of the cross section is different by a factor of around 2.5. At low energies the reaction cross section vanishes which is not in agreement with the measurements.

2.2.2 Total inelastic cross section

Besides the calculation of the reaction cross section also the total inelastic cross section for the different physics lists are calculated.

Equation 2.2 is modified. N_{Li} is replaced by the number of inelastic processes N_{Inel}. This number is determined by counting the number of events when the G4HadronInelasticProcess decides to act on an incoming Li-7. To save computing time the total number of events per job is reduced to one million events.

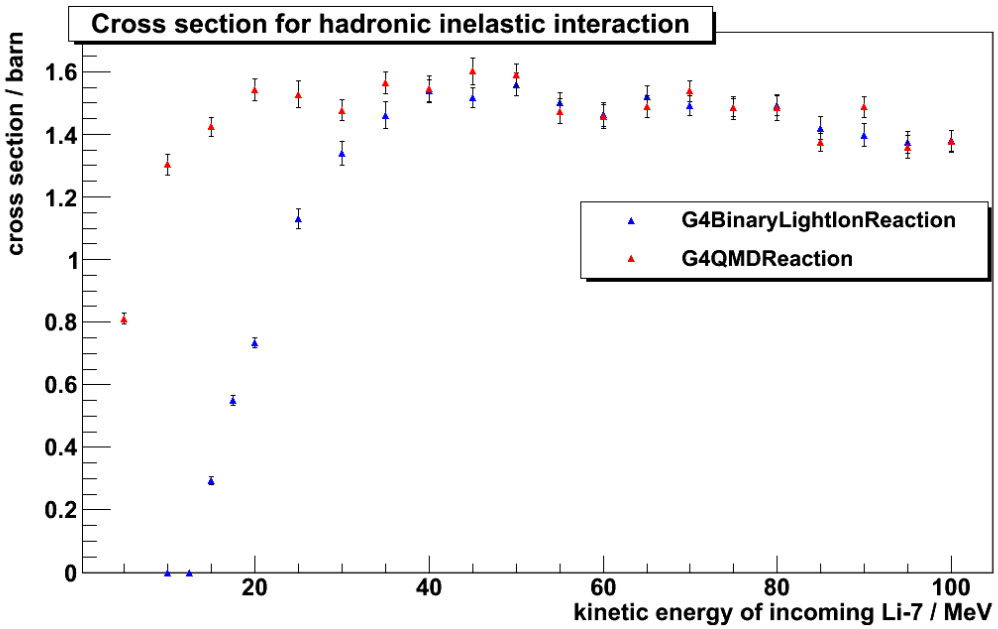

Figure 2.3: Total inelastic cross section as a function of the beam energy.

Figure 2.3 shows the result. Both physics list should use the same cross section models. The only difference is the usage of the Tripathi Light model in the prepared physics list for the G4BinaryLightIonReaction model. This cross section model should however not be valid for the reaction because the incident particle has an atomic number larger than two. Thus one would expect the same behaviour of the total inelastic cross section simply because both physics list contain the same models. The curves differ significantly from each other at low energies while they fit very well at higher energies. After a review of the model source code and a discussion with [5] it turns out that the Tripathi light model checks also the target material as incident particle. As a consequence the inelastic process uses for the G4BinaryLightIonReaction physics list the Tipathi light model which leads for lower energies to a different behaviour.

The Tripathi Light model delivers a cross section which vanishes at energies around 15 MeV. The cross section begins to fall significantly at energies of about 30 MeV. This could suppress the result of the reaction cross section. To avoid the early suppression at these higher energies and to use for both physics lists the same cross section models, the physics list for the G4BinaryLightIonReaction is rewritten without using the Tripathi Light model. With this new physics list the total inelastic cross section shows the same result, within statistical uncertainty, like the one which contains the QMD model. A suppression of the G4BinaryLightIonReaction model could now be excluded at energies around $10-30$ MeV.

At this point it would be necessary to compare the results for the total inelastic cross section with measurements. Unfortunately this is not possible at this stage. Measurements for the total inelastic cross section, if there are any at these energies, could not easily be compared with the simulations, [5]. To compare results it must be clear what exactly is measured and how the measurements are done.

It is a question of what the experimenter understand when he speaks of hadronic inelastic interaction and what type of reactions are included in the models of Geant4. To produce comparable results the simulation must contain the experimental setup. This is out of scope of a Bachelor thesis. Nevertheless this has to be done in the future. The results for the reaction cross section in section 2.2.1 can be compared because the reaction is well-defined.

The new physics list is used and the simulations for the reaction cross section are done again. Figure 2.4 shows the result of the new simulation in comparison with the older one which uses the Tripathi Light model. The suppression effect of the cross section model is visible at energies of 20 MeV and 25 MeV. The difference is not large and thus the fact that the reaction cross section calculated with the G4BinaryLightIonReaction model vanishes at lower energies is not reasoned by the cross section model.

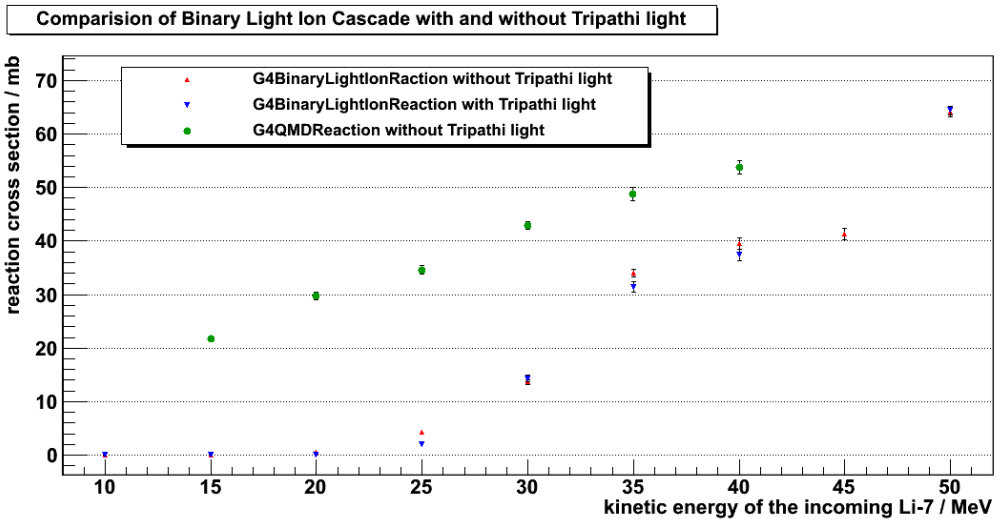

(a) Results for G4BinaryLightIonReaction with and without Tripathi light

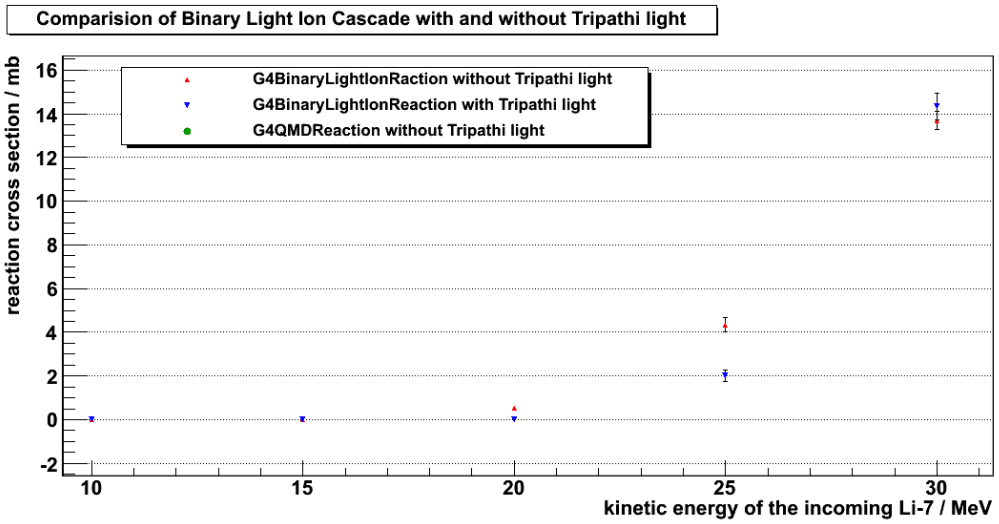

(b) The same as in the image above but a more detailed view.

Figure 2.4: Reaction cross sections with and without the Tripathi light model for the totel inelastic cross section.

Both models, or more accurately both physics lists, are in disagreement with the measurements. It is not possible to judge the behaviour of the total inelastic cross section without measurements. Consequently it is not totally clear if the wrong behaviour of the reaction cross section in comparison with measurements is only caused by the interaction models themselves. Possibly the cross section models show a completely wrong behaviour which leads to wrong reaction cross section results. Nevertheless both reaction models are not consistent with each other. This intensifies the suspicion that both models or at least one model could not be used at these energy regions without modifications and optimizations.

2.3 Kinematics

In addition to the investigation of the cross sections also the study of the kinematical results are interesting. Both models show a great deviation (see section 2.2) in the reaction cross section but they can still show good or understandable results in the kinematics. To explore the kinematics the production angle, the angle between the momentum directions of the outgoing Li-8 (or B-8) and the incoming Li-7 (Li-6), and the kinetic energy of the produced ions are calculated. The simulations start at energies in the validity range and the kinetic energy is decreased step by step to be able to see how the different models develop. To save computation time these simulations are done for the Li-8 production because the expected cross section of this reaction is much higher as the one for the B-8 production.

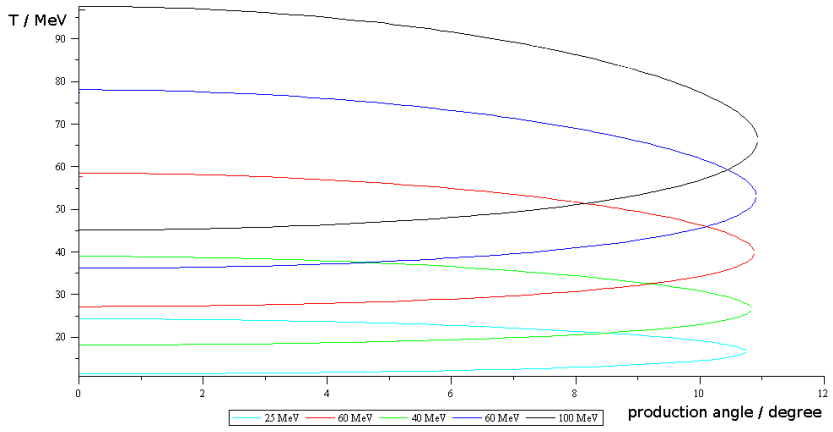

Figure 2.5: Theoretical expected behaviour from a four momentum calculation for five different incoming Li-7 beam energies.

The production angle and the kinetic energy of the produced Li-8 are related to each other. Thus a plot with production angle versus kinetic energy will show if the models have the same behaviour or not. In principle one would expect curves which are shown in figure 2.5. These curves are derived by a simple four momentum calculation in which the velocities of the target particles are set to zero and intra-nuclear momentum exchange is not considered.

Plot 2.6 shows the result of the Geant4 simulation for some selected incoming kinetic energies. On the left side the results for the G4BinaryLightIonReaction model are shown and on the right the one for G4QMDReaction. Both pictures seem to show a completely different behaviour. The G4BinaryLightIonReaction model reproduces the expected curves. Small statistical deviations are visible. This behaviour is the same for all the energies. The image for the incoming 25 MeV beam has less statistics than the one for 100 MeV because of the smaller reaction cross section in the model. The maximum production angle goes down with decreasing energies of the incoming Li-7 beam.

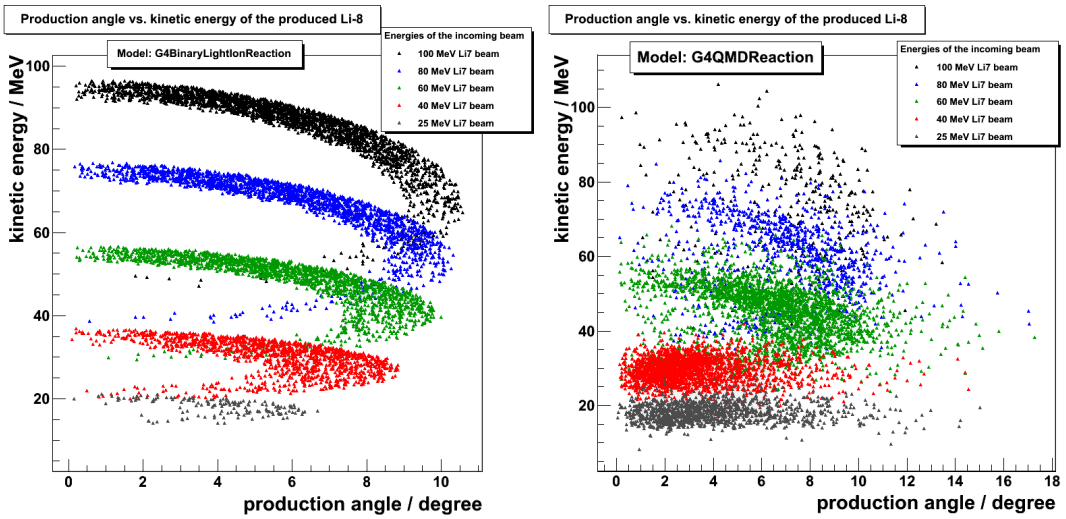

(a) G4BinaryLightIonReaction model

(b) G4QMDReaction model

Figure 2.6: Kinetic energy and production angle of the produced Li-8 ions simulated with Geant4 with different models

The results from the G4QMDReaction model look different. The expected curves reproduce at high energies (in this case $100 - 60\,\text{MeV}$). The statistical fluctuations are larger. The behaviour for lower energies shows a completely different image. No separation of the upper and lower energy branch is visible. To compare the results in a more detailed way histograms for the production angles and the kinetic energies are shown in figure 2.7 for $30, 60$ and $80\,\text{MeV}$.

The histograms confirm the first observation. For the G4BinaryLightIonReaction model the resulting distributions have nearly the same shape for the different energies. The G4QMDReaction model however shows a different behaviour: At higher energies, namely 60 and 80 MeV, the distribution have a similar shape like the one from the G4BinaryLightIonReaction. Both have their maximum at angles around $8 - 10\,°$. Furthermore the QMD model shows more statistical fluctuations which leads to the production of higher angles. These few events seems to be neglectable.

At lower energies of the incoming particle the distributions starts to differ: the peak of the histograms starts to shift to lower angles for the QMD model. At 30 MeV the distribution of the QMD model show a Rayleigh distribution like shape. This is a completely different result from the one of the binary cascade. To judge the different results measurements for the differential cross section are needed.

It is expected at these low energies that the QMD model, which seems to contain more detailed informations about intra-nuclear processes, should show better results, [5]. One expect in this case much more statistical fluctuations due to intra nuclear momenta of the nucleons than shown in the G4BinaryLightIonReaction model, [5]. Starting from these indications the behaviour of the QMD model could be more accurate at this energy level than the one of the binary cascade. Also the fact that the reaction cross section of the QMD model shows a peak like behaviour gives a little bit more confidence in the QMD model. This can of course not be the final answer without measurements.

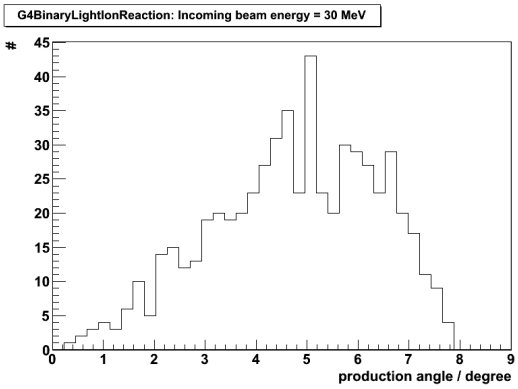

(a) G4BinaryLightIonReaction: 30 MeV

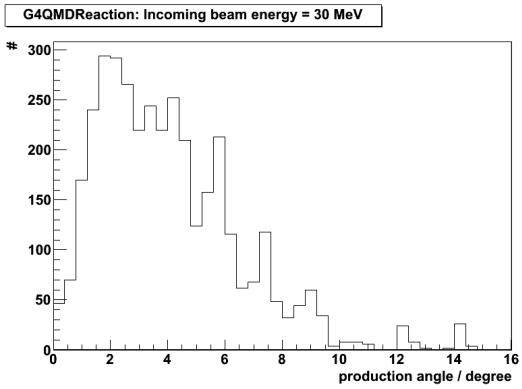

(b) G4QMDReaction: 30 MeV

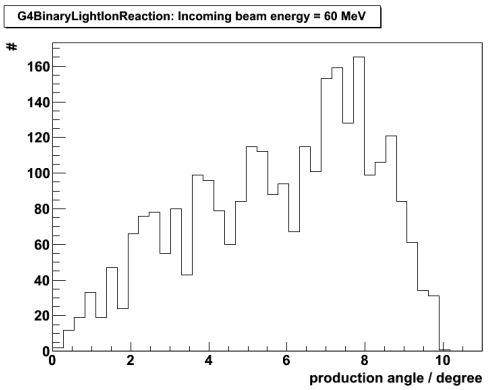

(c) G4BinaryLightIonReaction: 60 MeV

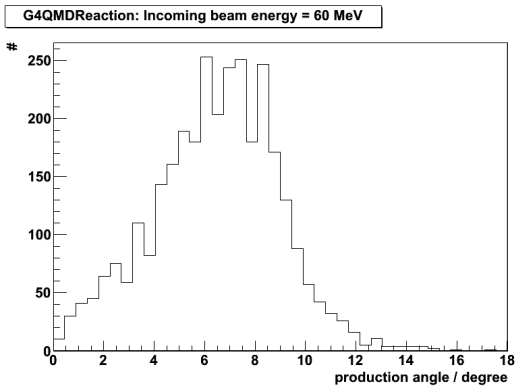

(d) G4QMDReaction: 60 MeV

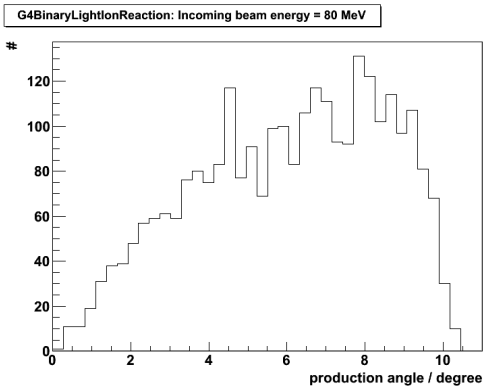

(e) G4BinaryLightIonReaction: 80 MeV

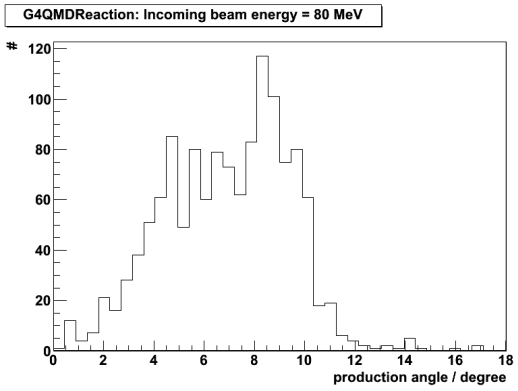

(f) G4QMDReaction: 80 MeV

Figure 2.7: Histograms of the production angle for the two models and different incoming beam energies

If the behaviour of the QMD model is correct for lower energies a problem for the production ring occurs. To have an efficient collection the ring capture device needs to cover the angular range where most of the Li-8 ions are produced. If the peak or mean value of the distribution is at very small angles the ring device has to cover this region. Thus the apperture for the circulating Li-7 becomes smaller. A too small apperture would decrease the beam lifetime significantly.

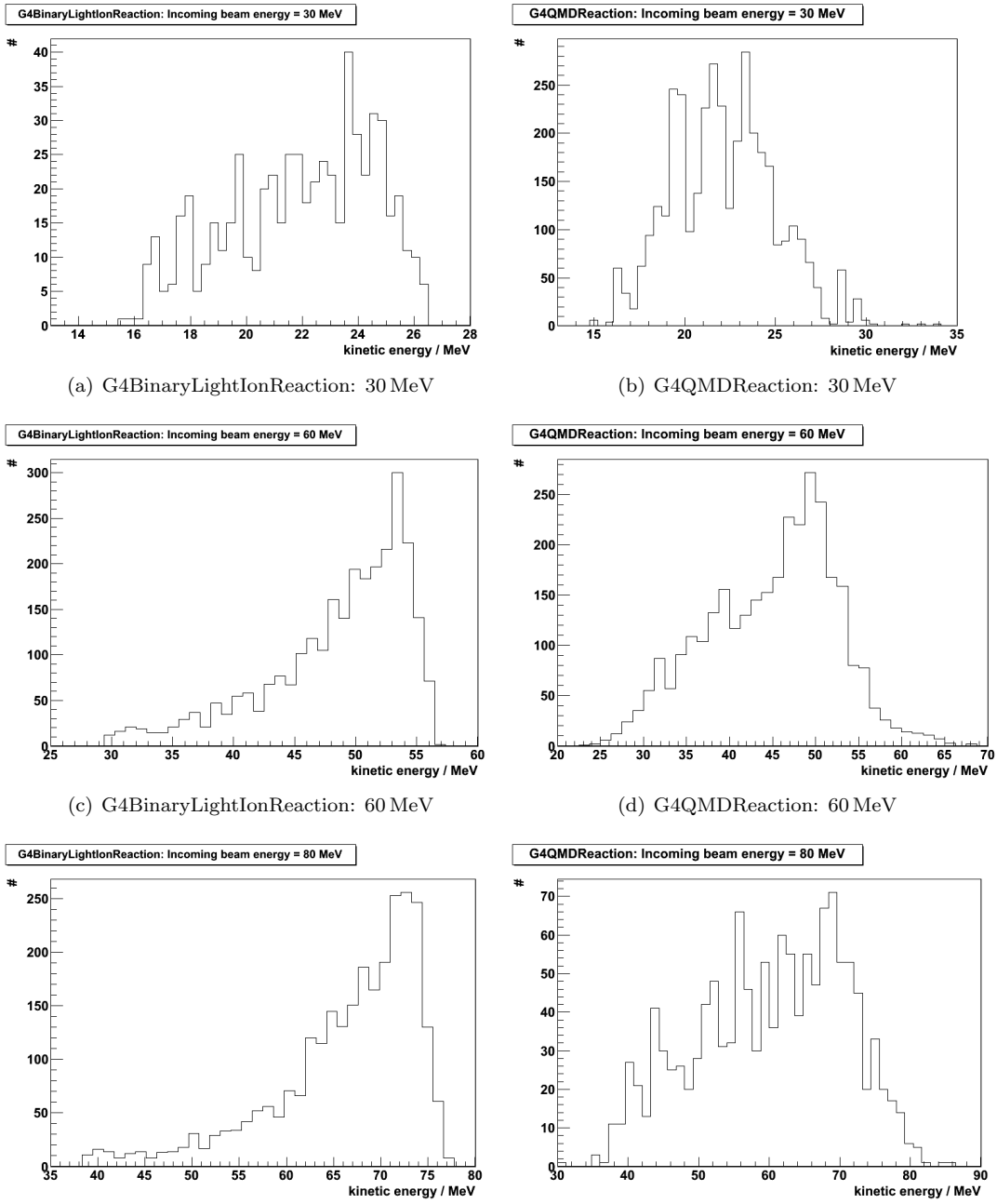

(a) G4BinaryLightIonReaction: 30 MeV

(b) G4QMDReaction: 30 MeV

(c) G4BinaryLightIonReaction: 60 MeV

(d) G4QMDReaction: 60 MeV

(e) G4BinaryLightIonReaction: 80 MeV

(f) G4QMDReaction: 80 MeV

Figure 2.8: Histograms of the kinetic energy of the produced ions for the two models and different incoming beam energies

To solve this problem the distance between gas jet target and the capture device has to be increased to separate the produced ions from the beam. Another possibility is to increase the angular distribution of the produced Li-8 by using septums or other magnetic lenses for separation. Nevertheless an angular distribution like this is of course not the favoured result. This consideration brings to mind that it is not enough for the production ring that the maximal production angle is small. Also the shape of the distribution is very important for the efficiency and the kind of realisation of the capture process.

Figure 2.8 shows histograms of the kinetic energy of the produced Li-8 ions for the different incoming beam energies, namely $30, 60$ and $80\,\mathrm{MeV}$. Again both models are not consistent. The binary cascade model is giving for the different incoming energies distributions with a peak at higher kinetic energies. The QMD model shows a similar distribution for high energies. For lower energies the shape of the distributions of the QMD model changes and seems to be different. The behaviour of the QMD model for small energies seems to switch completely. It is interesting to see that also energies above the incoming beam energies occur. This could be explained with intra-nuclear momenta of the nucleons which are also describes in the QMD model (Ref. [5]).

3 The ionization cooling

Beside the production of ions the gas jet target also has another task: It should provide cooling for the beam. As shown in section 1.4 there are two conditions which have to be fulfilled to allow a 6-d phase space cooling. Unfortunately these two conditions exclude each other. As a possible solution coupling between the different beam planes can be introduced. The partition number J_ϵ has to be increased to a positive value and the decrease of J_x needs to be counterbalanced on J_x and J_y. Below the condition for longitudinal cooling is studied.

3.1 Condition for longitudinal cooling

As mentioned in section 1.4 the fact, that a fast particle looses less energy than a slow one, needs to be corrected to make longitudinal cooling possible. The gas jet target needs a specific shape which provides a larger target thickness for particles with $\Delta p/p > 0$ than for particles with less momentum. To separate the particles according to their momentum deviation Δp, the dispersion D_x has to be non-zero at the point of the wedge. The dispersion provides an additional x offset:

$$x = D_x \cdot \frac{\Delta p}{p}$$

Therefore the target thickness needs to be increased for higher x values. The dispersion in y direction is zero. Thus the target should be translation invariant in this direction. The target is wedge shaped. Fig. 3.1 shows a sketch of the gas target. The shape of the target with the dispersion corrects the unwanted characteristics of the energy loss.

The geometrical parameter, defining the wedge, is the angle at the tip of the wedge, α. For large values of α the target thickness d, and therefore the thickness $t_h = \rho \cdot d$, is growing faster with x than for smaller α. Thus for a larger α, the displacement of the particles due to the dispersion does not have to be as large as for small α to reach the same energy loss behaviour with respect to the momentum dependence. The cooling condition can be fulfilled by choosing a large enough α for a certain dispersion. For a fixed value of α the dispersion has to be larger than a lower limit to fulfil the condition. The aim

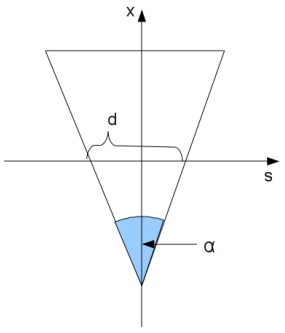

Figure 3.1: Sketch of the gas wedge target

of this chapter is to translate the abstract cooling condition

$$V = D_x \cdot \frac{\partial U}{\partial x} > -2 \cdot T \cdot \frac{\partial U}{\partial E} \tag{3.1}$$

into a useful geometrical condition which can be used to design a lattice with longitudinal cooling. T is the kinetic energy of the particle, U the energy loss in the wedge, E the total particle energy and D_x the dispersion in x direction. The minimum required target angle α_{min} needs to be calculated as a function of the dispersion or the minimum required dispersion is needed for a certain target angle.

3.2 Modelling the gas wedge

As mentioned in section 2.1.2 the speed of the molecules in the gas jet is neglected simply because there are no possibilities to describe a jet in Geant4. To form the wedge target a class of Geant4, describing trapezoids, is used. The geometrical parameters are taken from [1]. A deuterium gas has a density of about $0.18\,mg/cm^3$ at normal conditions. To reach an energy loss of about 300 keV for a 25 MeV particle, the target needs a thickness t_h of the order of $300\,\mu g/cm^2$. This corresponds to a target thickness d of the order of 1.6 cm. For technical reasons a target thickness of about 5 cm is preferred. The gas density is reduced to hold the thickness t_h for a thicker target.

A particle on orbit passes through the center of the gas jet. It sees a fixed thickness of 5 cm. The gas pressure and density are adjusted to generate an energy loss of $300\,keV$ at $25\,MeV$ incident energy. According to eqn. 1.15 a thickness of $280\,\mu g/cm^2$ is needed. The height of the target is set to an artificially high value ($1\,m$).

3.3 Simulation of the energy loss

To study the cooling condition, fully striped Li-7 ions are simulated with Geant4 at a certain energy. One Li-7 ion is generated per event. It traverses the gas wedge and the energy loss in the target is recorded.

To study the longitudinal cooling condition 3.1, derived by [1, 2], V has to be calculated out of Geant4 simulations for different setup parameters like the angle of the wedge, beam energy, target thickness or dispersion. V is not directly calculable, but a similar variable:

$$U = U(p, x) \tag{3.2}$$

$$\Rightarrow \quad U \approx U_0 + \frac{\partial U}{\partial x}\Delta x + \frac{\partial U}{\partial p}\Delta p \tag{3.3}$$

$$\text{with} \quad \Delta x = D_x \cdot \frac{\Delta p}{p} \tag{3.4}$$

$$\Rightarrow \quad U \approx U_0 + \underbrace{\left[\underbrace{\frac{\partial U}{\partial x} \cdot D_x}_{=:V} + p \cdot \frac{\partial U}{\partial p}\right]}_{=:S} \cdot \frac{\Delta p}{p} \tag{3.5}$$

With momentum deviations introduced the energy loss in the target should have a linear dependence on $\Delta p/p$ as long as its small. The slope of the straight line is S.

In the simulations different values of the relative momentum deviation $\Delta p/p$ are assumed. The energy loss in the wedge target is calculated for each of the different $\Delta p/p$. V is not directly accessible

because the second term in the slope S of the energy loss, containing $\partial U/\partial p$, is non-zero. Only the slope S is directly calculable and therefore the cooling condition 3.1, containing V, should be transformed to a condition for S:

$$V + 2 \cdot T \cdot \frac{\partial U}{\partial E} > 0 \tag{3.6}$$

$$\text{with} \quad \delta E = \frac{2T}{p} \cdot \delta p \quad \text{cf. [2] (non-relativistic)} \tag{3.7}$$

$$\Rightarrow \quad V + p \cdot \frac{\partial U}{\partial p} = S > 0 \tag{3.8}$$

Thus the cooling condition is expressed for the parameter S which has to be larger than zero.

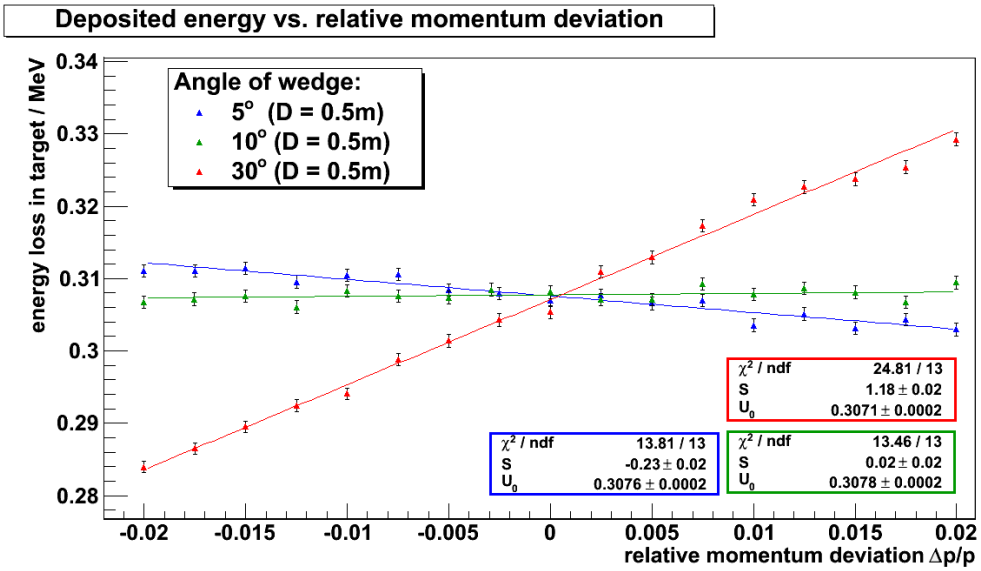

Figure 3.2: Momentum dependent energy loss for different wedge angles ($\alpha = 5°, 10°, 30°$) but for the same dispersion

The momentum of the incident Li-7 particle is changed step by step from -2% to $+2\%$ of the mean momentum. For each momentum step the x offset of the particle is calculated from the assumed dispersion D_x. Betatron oscillations around the dispersion orbit are neglected because by averaging over many turns in the ring the mean x position of the particle should be equal to the x offset of the dispersion orbit compared to the design orbit. One thousand events with one particle each are simulated for each setup. The energy loss is calculated for each event. After that the mean value and its error is computed. The results are shown in figure 3.2. As expected the energy loss shows a linear dependence on $\Delta p/p$.

Simulations are done for angles of the wedge between 2.5° and 100° for different values of the Dispersion. Fig. 3.2 shows three angles for a fixed dispersion of 0.5 m. As expected the slope becomes larger with growing angle due to the growing $\frac{\partial U}{\partial x}$. If the angle reaches a certain value (in this case around 10°) the slope of the straight line S becomes positive. This is the point where a too fast particle starts to loose more energy than a slower one. At this critical point longitudinal phase space cooling becomes possible.

The value of S is determined by fitting function 3.5 to the data via the χ^2 method. The resulting

χ^2/ndof are around $1-2$ demonstrating the validity of the linear approximation. Then the value of S is plotted against the angle of the wedge for dispersions between 10 cm and 1 m. Figure 3.3 shows three examples.

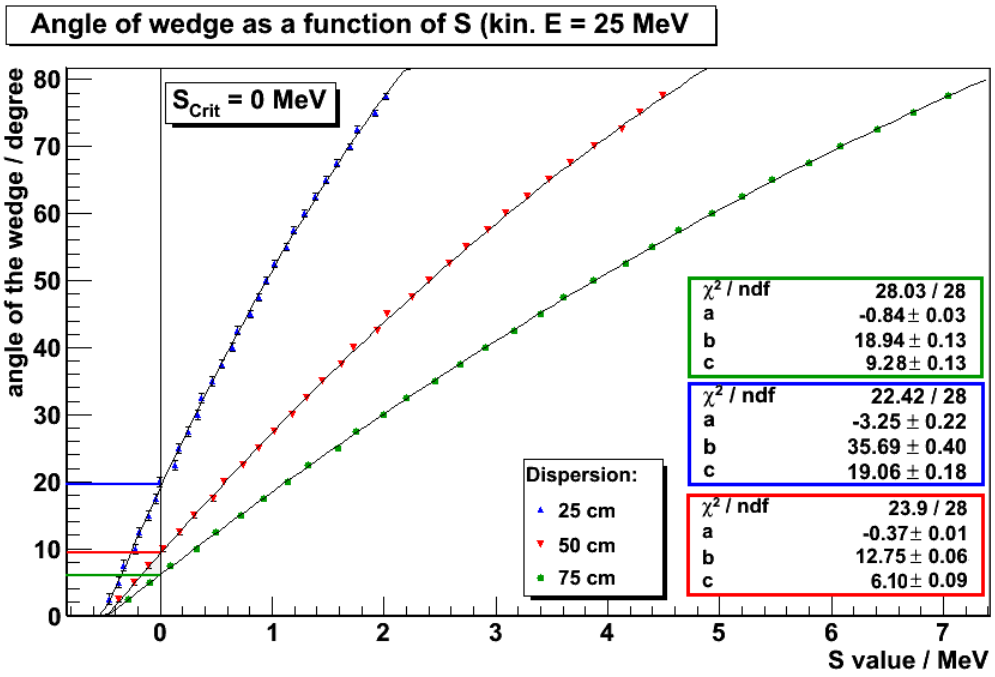

Figure 3.3: Wedge angle α as function of S for three different assumed values of the dispersion.

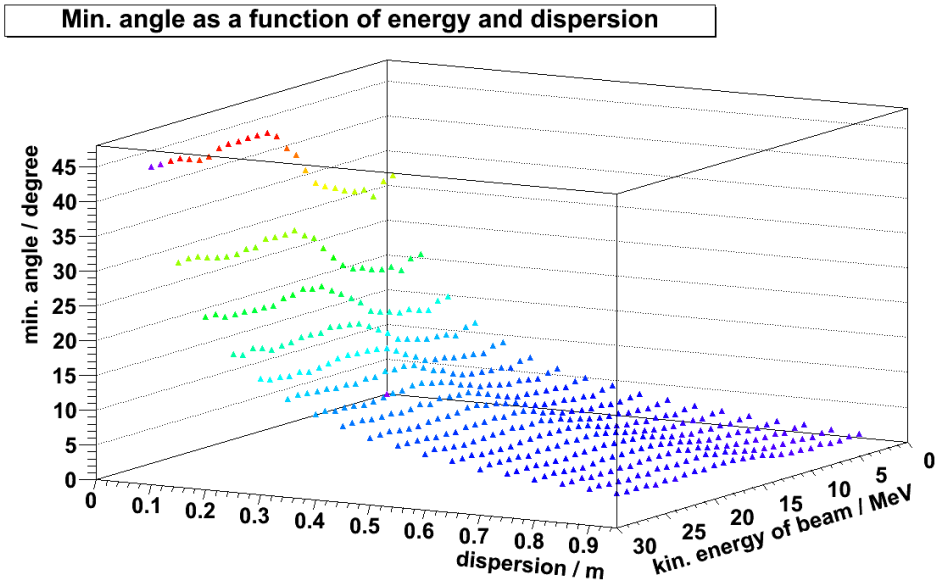

Figure 3.4: Minimum required angle of the wedge as a function of dispersion and beam energy (thickness of the wedge $0.280 mg/cm^2$)

S needs to be larger than zero. To calculate the critical angle α_{min}, which correspond to $S = 0$, and to estimate its error a χ^2 fit is done of the following form:

$$\alpha(S) = a \cdot S^2 + b \cdot S + c$$

The resulting χ^2/ndof are around one. By using $S = S_{crit} = 0$, α_{min} can be derived as a function of the dispersion. The critical angle α_{min} is the minimum required angle. Also larger angles for the same dispersion would fulfil the cooling condition.

Up to now the incoming beam energy was 25 MeV. To study the requirements for other incoming beam energies, the kinetic energy T is changed step by step from 5 MeV up to 30 MeV. For each beam energy the minimum required angle is calculated as a function of the dispersion with the same method. Finally the minimum required wedge angle is derived as a function of the dispersion and the incoming beam energy. Plot 3.4 shows the result of the calculation.

In addition to that the other parameters of the wedge could be changed namely the density of the gas jet and the thickness d of the wedge at the point where an ideal particle traverses the target. Figure 3.5 shows different curves of the minimum required angle as a function of the dispersion. For the first simulation the thickness was chosen to 280 $\mu g/cm^2$ with a corresponding energy loss of 300 keV for a 25 MeV beam (blue line). Assuming a wedge angle of 20° the lattice has to provide a dispersion of at least 24 cm.

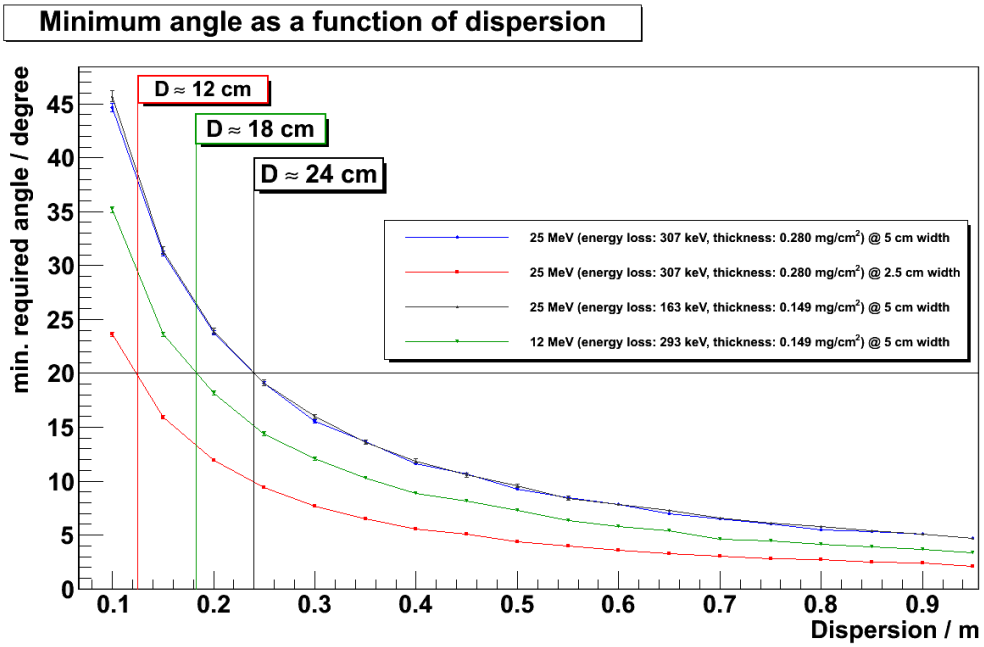

Figure 3.5: Minimal required wedge angle as a function of dispersion for different target properties. $\alpha - D$ pairs above the lines fulfil also the longitudinal cooling condition.

As a next step the effective thickness t_h at nominal impact is kept, but the physical thickness d is reduced from 5 cm to 2.5 cm. The density of the gas is increased by a factor of two. One would expect that the requirements for the wedge angle becomes weaker due to the fact that the energy loss for a faster particle, which is arriving at a certain x offset (dispersion), will increase much stronger because of the higher density. Simply the thickness is growing faster with the x offset of the particle for the same wedge angle. The simulation for this setup (red line) confirms the expectations. For this scenario and

a chosen wedge angle of 20° a dispersion of at least 12 cm are needed. A growth of the target thickness d by a fixed target thickness t_h would have the opposite effect namely the requirements become stronger.

If the thickness of the target is kept, slower particles will loose more energy than faster ones. A 12 MeV particle for example has an approximately energy loss of about 650 keV. To get for a particle like this a 300 keV energy loss the thickness needs to be reduced to a value of about 150 $\mu g/cm^2$. This is done in a simulation where a target thickness of 5 cm is chosen. Consequently the gas density is reduced. The green line shows the result for a 12 MeV particle with an energy loss of 300 keV and the dark gray line the one for a 25 MeV particle with an energy loss of about 160 keV.

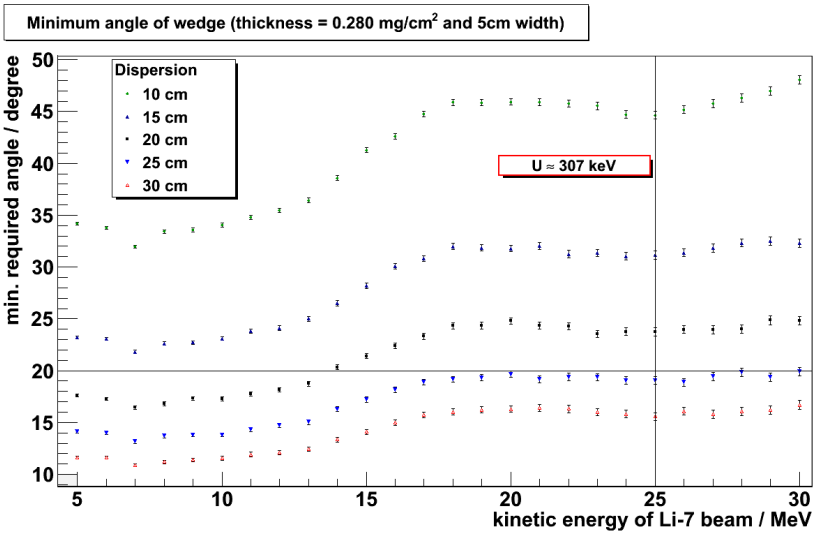

(a) Thickness: 280 $\mu g/cm^2$

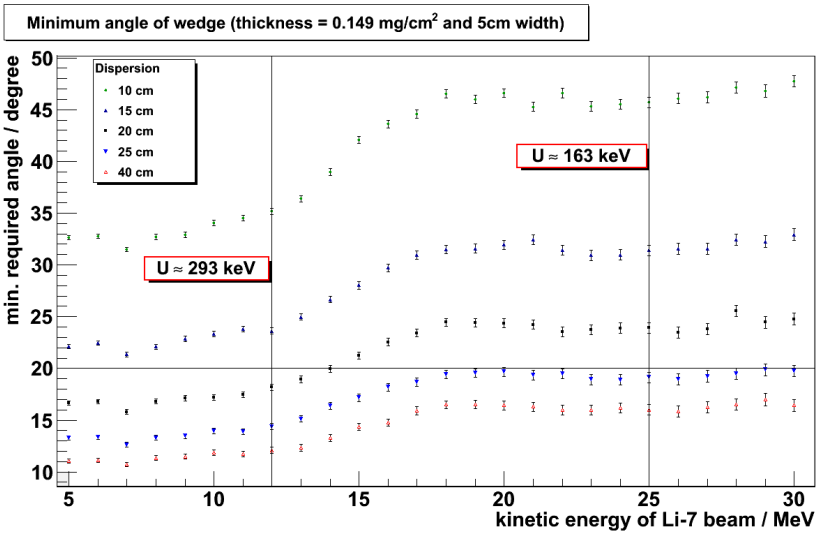

(b) Thickness: 149 $\mu g/cm^2$

Figure 3.6: Energy dependence of the critical wedge angle for two different parameters

A 25 MeV particle for this scenario produces the same result like the one for the original setup (t_h:

$0.28\,mg/cm^2$, d: 5 cm). One could expect in this case that the restrictions for the minimum required angle are stronger because of the smaller gas density. Therefore a larger angle should be needed. By looking at the definition of S, it becomes clear that S is proportional to derivatives of the energy loss U, namely $\frac{\partial U}{\partial x}$ and $\frac{\partial U}{\partial p}$. Those derivatives are approximately proportional to the thickness t_h and thus also S is proportional to the thickness t_h. S should be larger than zero. This means that the cooling condition is approximately independent from the thickness t_h. As a result the thickness t_h of the target can be varied to reach a certain energy loss without changing the angle and dispersion requirements if the target thickness d is kept.

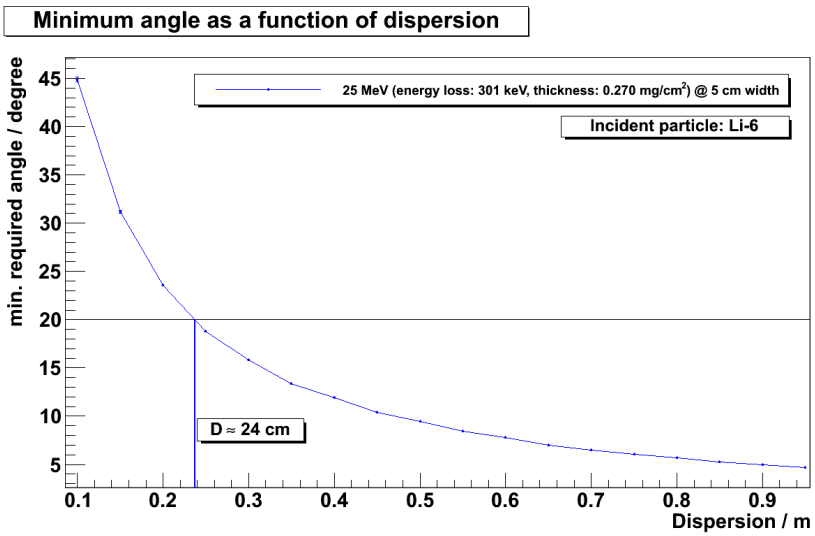

(a) α as a function of dispersion

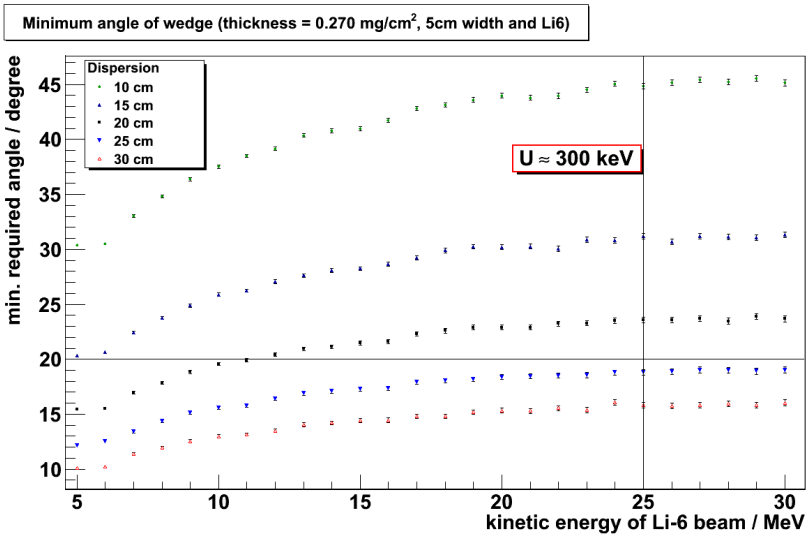

(b) α as a function of energy

Figure 3.7: Critical angle of wedge as a function of dispersion and energy for a $270\,\mu g/cm^2$ target

If the target thickness d is varied, the angle requirements will change as seen above. This is caused by the d dependence of $\partial U/\partial x$. By changing only d, $\partial U/\partial x$ is changed and therefore the cooling require-

ments have changed. A 12 MeV particle in this scenario looses 300 keV. The minimal angle is different from the 25 MeV particle due to the energy dependence of the minimum required angle. The energy dependence for different dispersion values is shown in figure 3.6.

In addition to these Li-7 simulations also the results for a Li-6 beam for the B-8 production is studied. A thickness of about $270\,\mu g/cm^2$ and $d = 5$ cm are chosen to get an 300 keV energy loss for a 25 MeV particle. The results show nearly the same behaviour and can be studied in figure 3.7.

The condition for longitudinal cooling is studied and translated into simple requirements which are needed for a lattice design or for the design of the gas jet target. The results of the simulations are used by [3] for the lattice design to ensure a dispersion at the target position which is large enough. A wedge angle of 20° is assumed and therefore a dispersion larger than 24 cm.

3.4 Condition for $J_\epsilon = 0.13$

To obtain cooling in all dimensions, the different phase spaces need to be coupled. [2] suggests a solenoid to get for each partition number a value of $J_i = 0.13$. With the simulations results above it is possible to calculate the required wedge angle as a function of the dispersion to obtain $J_\epsilon = 0.13$.

$$\alpha_\epsilon = J_\epsilon \cdot \frac{f_s U}{2T} = \frac{f_s}{2} \cdot \frac{\partial U}{\partial E} \tag{3.9}$$

$$\text{with} \quad \frac{\partial U}{\partial E} = \underbrace{\left(\frac{\partial U}{\partial E}\right)_0}_{=\frac{p}{2T}\frac{\partial U}{\partial p}} + \frac{V}{2T} \tag{3.10}$$

$$\Rightarrow 2 \cdot J_\epsilon \cdot U = V + p\frac{\partial U}{\partial p} = S \tag{3.11}$$

With $J_\epsilon = 0.13$ and $U = 0.3$ MeV, S has to be around 0.078 MeV.

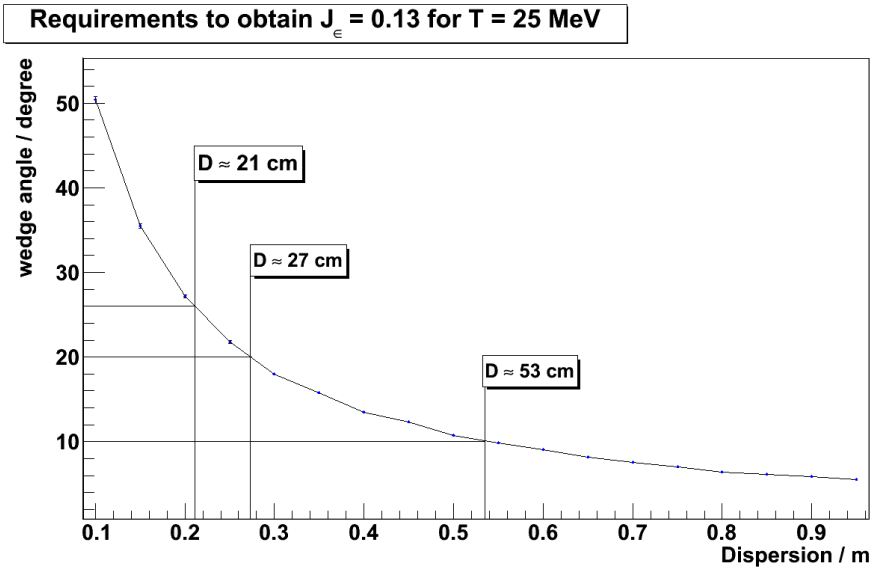

Figure 3.8: The wedge angle α as a function of the Dispersion D_x. For each point on the line, one obtain $J = 0.13$.

By using the simulated data and $S_{crit} = 0.078\,\text{MeV}$, α is computed as a function of D_x. The curve in image 3.8 describes the $\alpha - D_x$ pairs which allow $J_\epsilon = 0.13$. A target thickness of $0.28\,mg/cm^2$ with $d = 5\,\text{cm}$ and a kinetic energy of $25\,\text{MeV}$ is chosen.

Assuming a wedge angle of $10°$, the dispersion has to be around $53\,\text{cm}$. For $\alpha = 20°$ a dispersion of $D_x = 27\,\text{cm}$ is needed.

4 Tracking

The considerations above might have left the impression of a static situation but the scattering process and the energy loss in the target is a statistical process. To study the whole cooling and heating concept in a more realistic framework and to verify the results from the simulations above the production ring needs to be simulated with a tracking code. A tracking code calculates the motion of one or more particles through a predefined lattice. Due to the fact that a cavity is involved to compensate the energy loss, the tracking code has to be 6-dimensional: it is necessary to know when and therefore at which phase the particle is arriving at the cavity. Thus $\Delta p/p$ (fifth dimension) and Δt (sixth dimension) need to be tracked. There are several tracking codes providing 6-d tracking but none of them has an element included, describing a gas jet target. An existing code has to be extended by a gas target element.

4.1 Representative target model for sixtrack

A simple model of a gas target has to be introduced into an existing tracking code. The first idea was to replace the target by a simple kick. A particle penetrating the target changes its directions x' and y', but not its vertical and horizontal positions. In addition to that it will loose energy. To take into account the statistical behaviour of the kink, it is based on a random generator. But we need to know the statistical distributions of the kink angles and energy loss. These can be derived from the Geant4 simulations presented in the previous chapter.

4.1.1 Angular distributions

One would expect for x' and y' a gaussian like distribution with a mean value of zero and a certain RMS (cf. [12]). The RMS value depends on the thickness of the target and the energy of the particle. But there are non-gaussian tails. The gaussian part of the distribution covers only about 98% of all scatters [12].

The images 4.1 show the result of a Geant4 simulation for a 25 MeV Li-7 beam and a target thickness of $0.28\,mg/cm^2$. As expected the distributions of x' and y' are gaussian-like with a zero mean value.

Introducing spherical coordinates with the total scattering angle θ (angle between momentum direction before and after the target) and ϕ, the angle in the $x' - y'$ plane measured against the x' axis. The Geant4 simulations show a uniform distribution for ϕ (the scattering process does not prefer a certain direction) and a Rayleigh distribution for θ.

As a result the scattering angle can be approximately simulated by generating a uniform distribution for ϕ and a Rayleigh distribution for θ which could be done simply by the transformation method. Alternatively two gaussian distribution can be used to reproduce the behaviour of the Geant4 simulations.

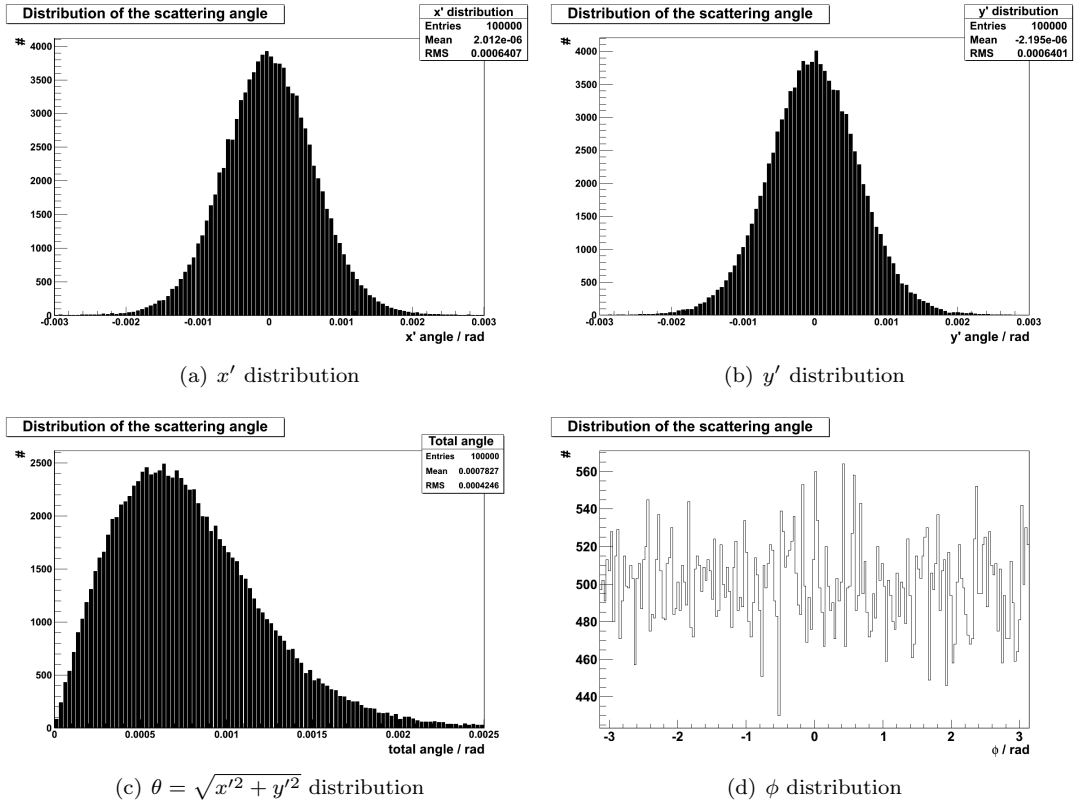

(a) x' distribution

(b) y' distribution

(c) $\theta = \sqrt{x'^2 + y'^2}$ distribution

(d) ϕ distribution

Figure 4.1: Geant4 simulations for the scattering behaviour (25 MeV beam and 280 $\mu g/cm^2$ thickness)

There are serveral formulae to calculate the RMS angle of the distributions. A formula from PDG [12] is used here:

$$\sigma = \frac{a \cdot \text{MeV}}{\beta \cdot cp} z \sqrt{\frac{x}{X_0}} \cdot \left[1 + 0.038 \ln\left(\frac{x}{X_0}\right)\right] \tag{4.1}$$

$a = 13.6$ is a parameter extracted from measurements. p, βc and z are the momentum, the velocity and the charge of the incident particle. x is the thickness of the target (in this case around $0.28\, mg/cm^2$) and X_0 the radiation length. The accuracy of the formula for singly charged particles with $\beta \approx 1$ and ratio x/X_0 within $[10^{-3}, 100]$ is 11% or better. X_0 is for a deuterium gas approximately $127\, g/cm^2$ (using the Dahl formula in [12]). Thus the ratio x/X_0 is of the order of $2 \cdot 10^{-6}$ which is significantly below the range of validity of equation 4.1.

To test the formula, the angular distributions are determined by simulating 10^5 incoming events for different thickness and beam energy setups. The RMS and its error are calculated. The thickness is varied from around $0.265\, mg/cm^2$ to $0.295\, mg/cm^2$ for three incident energies: 24.5 MeV, 25 MeV and 25.5 MeV. To check the energy dependence the energy is varied within 24 MeV and 26 MeV for a thickness of $280\, \mu g/cm^2$.

There is no good agreement between formula 4.1 and the Geant4 data (see figure 4.2). This is no surprise. The ratio of x/X_0 is out of the validity range, the particles have a charge of $+3e$, the relativistic β is around 0.09 and also the value of X_0 is only approximately determined. In the following it is assumend that Geant4 is working well.

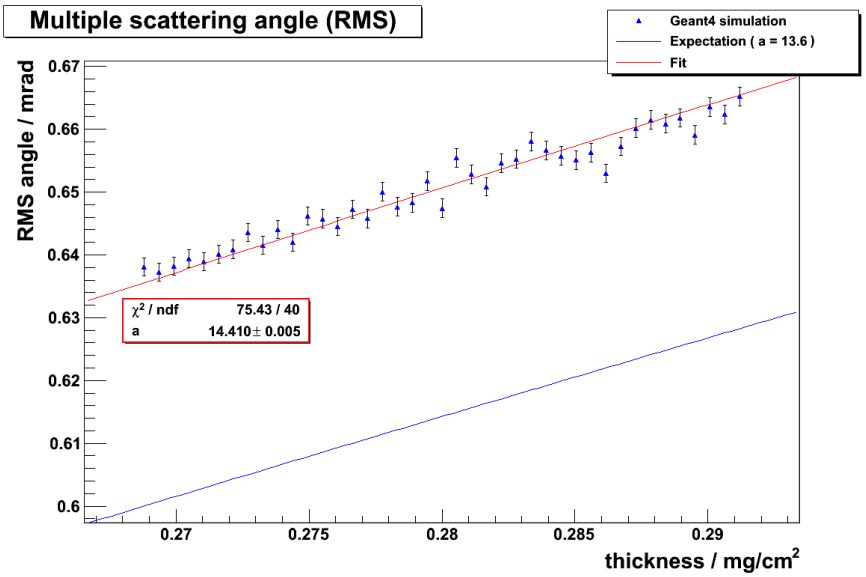

(a) Thickness dependence of the RMS angle

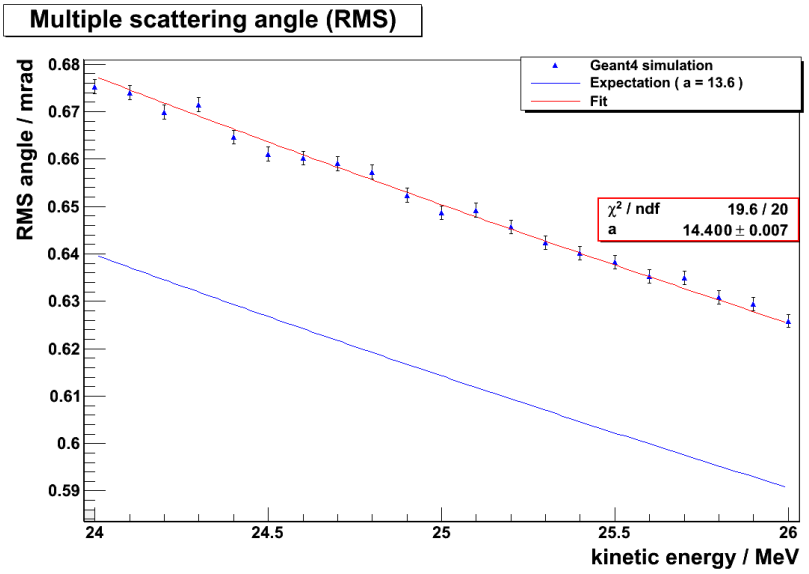

(b) Energy dependence of the RMS angle

Figure 4.2: Comparison of the Geant4 simulated data and eq. 4.1. The blue line shows the uncorrected formula and the red one the results of a χ^2 fit.

The parameter a is readjusted by a χ^2 fit to the simulation. Figure 4.2 illustrates two ways of doing the fit. They give compatible results.

Figure 4.3 shows the fits for the different beam energies. The resulting values for a only differ by 0.1%. A unique value of 14.41 is used for all beam energies.

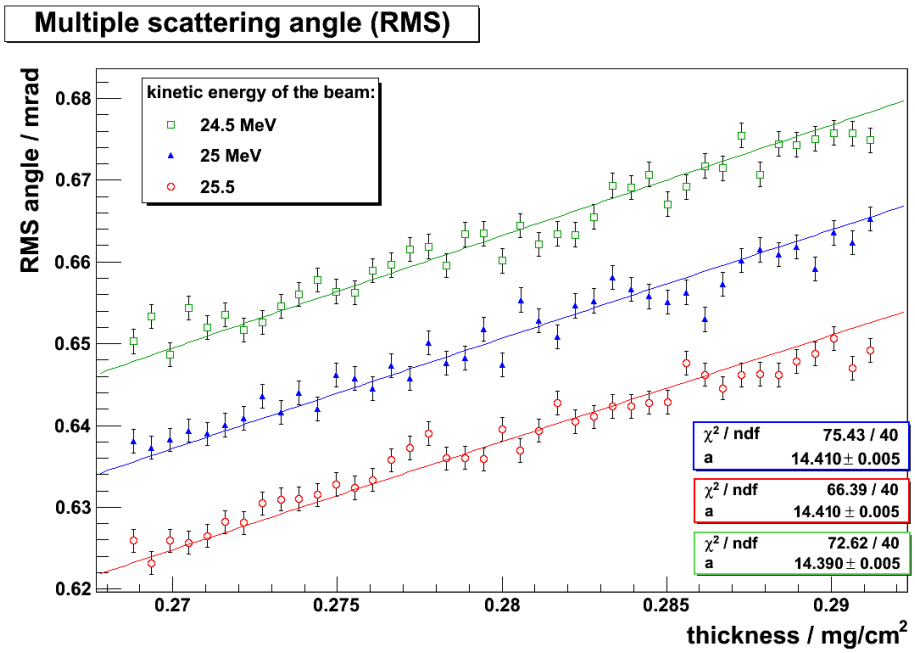

Figure 4.3: RMS scattering angle as a function of the thickness for different energies. The coloured lines show the result of χ^2 fits.

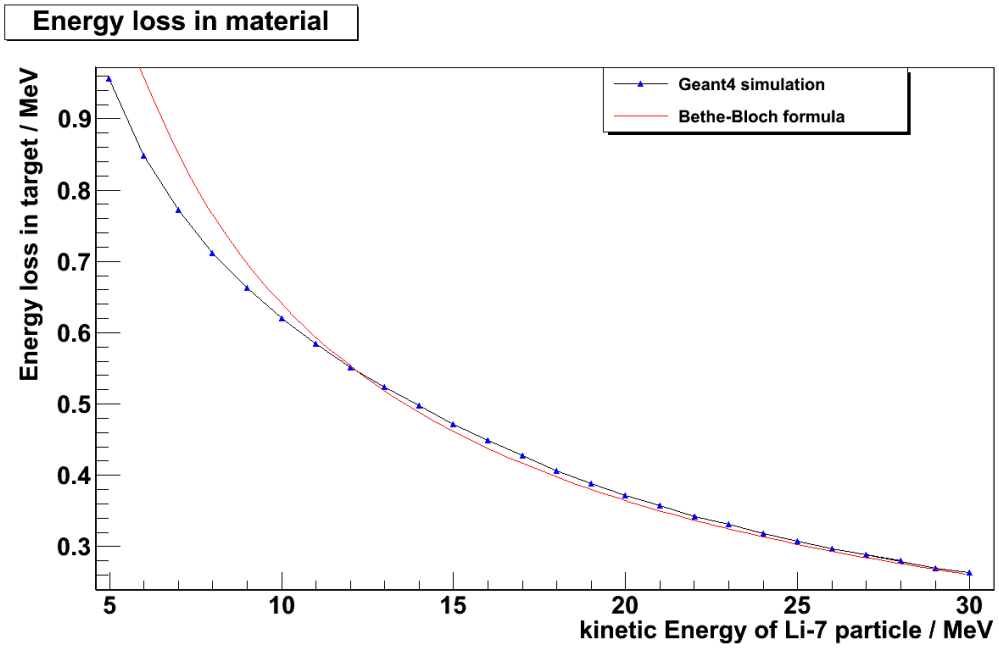

Figure 4.4: Comparison between the Bethe-Bloch equation and a Geant4 simulation

4.1.2 Energy loss distribution

To simulate the energy loss in the target, the results of the Geant4 simulations of section 3 are used. The distribution of the energy loss is gaussian and therefore the mean value and the distribution width is needed. A first idea to calculate the mean value is to use the Bethe-Bloch formula. Figure 4.4 shows a comparison between the results of the Geant4 simulations and the Bethe-Bloch formula. For the analytic calculation the energy loss at the initial energy is simply multiplied with the thickness of the target. Above 10 MeV this works fine and the result is used as a first approximation. An analysis showed no simple distribution. Instead a gaussian with an RMS of 0.0271 MeV will be used.

These parameters are used to implement the model in sixtrack, a full 6-d tracking code. The target is replaced by an infinitesimal thin foil which is only providing a kick and energy loss to the particle. A change of the particle position in x and y and a time delay due to the scattering is neglected. The implementation and the tracking simulation in the modified sixtrack is done by Michaela Schaumann in [3].

4.2 Implementing a tracking code

Here I take a different approach. A tracking code is written in C++ and included in a Geant4 simulation. Now the full Geant4 simulation is available.

4.2.1 General requirements and program structure

As already mentioned above there are certain requirements for the new tracking code. The code needs to do a full 6-d phase space tracking (the coordinates $x, x', y, y', \frac{\Delta p}{p}, \Delta t$).

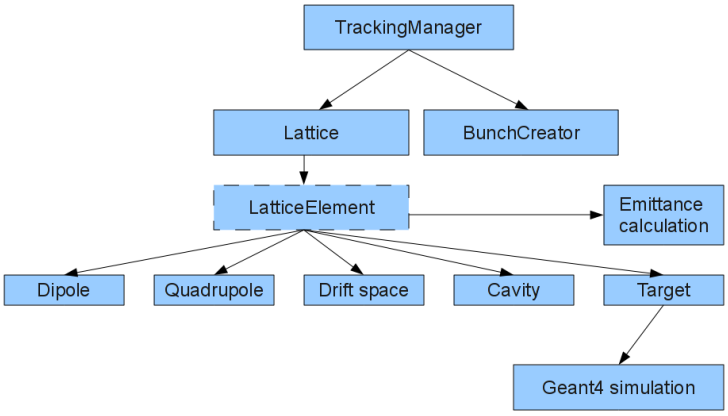

Figure 4.5: Simplified structure of the written tracking program. Each blue box represents a C++ class. The whole Geant4 simulation of the target is capsuled in the target class.

The lattice of the ring, studied in [3], should not be hard-coded in the tracking code. Instead the structure and the strength of the lattice elements will be read from a simple and understandable "lattice description" file. This creates a technical independence of the tracking code and the lattice design. It is simple to add new lattice elements like sextupoles by introducing a new class of lattice element into the code. The code is written in an object-oriented language and style where each lattice element (dipole, quadrupole, cavity, target etc.) is implemented in a single class. These classes contain the element specific tracking code. On top of these classes there is a management structure which implements a parser to read the lattice structure and to create a list of lattice element objects. It also contains a

bunch creator to create a statistical distribution of the particles in the phase space and a tracking manager to control design parameters of the production ring (What kind of particle? Which design energy? Charge etc.). Figure 4.5 illustrates the structure of the program.

The boxes represent the C++ classes. The class "LatticeElement" is virtual. It describes a formal structure which all derived classes, containing the lattice element descriptions, must have. The target class is encapsulating a whole Geant4 simulation. The tracking code and the target simulation are related through one connection. Thus the tracking code is independent from the specific Geant4 simulation properties like for example the shape of the wedge. There is also a class to calculate the emittances of the bunch in a specific point of the lattice. The user of the program is able to determine the emittances simply by adding an "emittance print out point" in the lattice description file.

The advantage of the usage of virtual classes is clear: The superior management class does not have to know the different flavour of classes. Each lattice element looks the same to the management classes. As a result a new type of element, for example a sextupole, can be introduced without changing source code in the management structure.

The tracking code has to track more then one particle because statistical processes and quantities must be studied.

All the tracking implementations of the different lattice element types needs to be symplectic. If M is the matrix or map to track the particle's coordinates through an element, M is symplectic if the following condition is fulfilled, [13]:

$$M^T \cdot S \cdot M = S \tag{4.2}$$

$$\text{where} \quad S := \begin{pmatrix} 0 & 1 & 0 & 0 & 0 & 0 \\ -1 & 0 & 0 & 0 & 0 & 0 \\ 0 & 0 & 0 & 1 & 0 & 0 \\ 0 & 0 & -1 & 0 & 0 & 0 \\ 0 & 0 & 0 & 0 & 0 & 1 \\ 0 & 0 & 0 & 0 & -1 & 0 \end{pmatrix} \tag{4.3}$$

Symplecticity means conservation of phase space and therefore, [13]:

$$\lim_{n\to\infty} M^n = \text{finite} \quad \Rightarrow \quad \det M = 1$$

Other influences on the particles like for example space charge are neglected at this stage.

4.2.2 Assumptions and approximations

To implement a tracking code, one would solve the equation of motion for each magnetic element with symplectic numerical methods like Lie transformations, which are in most cases symplectic. An implementation based on Lie transformations is beyond the scope of this thesis.

Instead I implemented a kick code: the magnetic elements are replaced by thin lenses. This means that for example a quadrupole with a length l is replaced by a drift space of the length $l/2$, a kick with no length which provides only a change in the direction x' and y' and another drift of the length $l/2$. The smooth trajectory of the particle is replaced by a kink. In the following the implementation of the elements is explained.

The transportation of a particle through an element is done in most cases with a matrix multiplication:

$$\begin{aligned} \vec{z} &= \left(x, x', y, y', \frac{\Delta p}{p}, \Delta t\right)^T \\ \vec{z}(s_0 + l) &= M \cdot \vec{z}(s_0) \end{aligned}$$

Here M is a lattice element's specific transport matrix, s_0 the position in front of the element and $s_0 + l$ the position after the element. l is the length of the element.

Drift: The simplest element of a lattice is a drift space between the magnetic elements. The particle does not see any electromagnetic field and thus it does not change its direction. The new position after traversing the drift space can be calculated with the following transport matrix, [4]:

$$M_{Drift} = \begin{pmatrix} 1 & l & 0 & 0 & 0 & 0 \\ 0 & 1 & 0 & 0 & 0 & 0 \\ 0 & 0 & 1 & l & 0 & 0 \\ 0 & 0 & 0 & 1 & 0 & 0 \\ 0 & 0 & 0 & 0 & 1 & 0 \\ 0 & 0 & 0 & 0 & 0 & 1 \end{pmatrix}$$

Here l is the length of the drift space. The matrix does not change the momentum or the time delay. This is correct for the momentum but not for the time delay. After using the transport matrix, an additional δt is calculated by simple mathematics:

$$\delta t = \frac{\sqrt{l^2 + (x(s_0 + l) - x(s_0))^2 + (y(s_0 + l) - y(s_0))^2}}{v} - t_s$$

t_s is the time a synchronous particle will need for the drift space, v is the velocity of the current particle and s_0 the position in the ring where the drift space is starting. The new time delay Δt is corrected by δt.

$$\Delta t(s_0 + l) = \Delta t(s_0) + \delta t$$

Quadrupoles: As already mentioned above the quadrupoles are approximated by thin lenses. The first half of the quadrupole length is a drift space. Then the particle gets a kick, described for a focusing quadrupole (in the horizontal plane) with the following matrix, [4].

$$M_{QF} = \begin{pmatrix} 1 & 0 & 0 & 0 & 0 & 0 \\ -1/f & 1 & 0 & 0 & 0 & 0 \\ 0 & 0 & 1 & 0 & 0 & 0 \\ 0 & 0 & 1/f & 1 & 0 & 0 \\ 0 & 0 & 0 & 0 & 1 & 0 \\ 0 & 0 & 0 & 0 & 0 & 1 \end{pmatrix}$$

where $f = \frac{1}{k \cdot l}$ is the focal length of the quadrupole, k its strength. The strength itself is a function of the momentum and is corrected for each particle:

$$k = \frac{1}{1 + \frac{\Delta p}{p}} \cdot k_0$$

k_0 is the nominal strength of the quadrupole for the synchronous particle. After the kick, where no change in momentum and time delay is introduced, the particle is transported with a drift space of the length $l/2$ to the end of the quadrupole.

Dipoles: The description of the dipoles is more complicated. A transport matrix to calculate the particle's position after the dipole exists. This matrix is not symplectic and can only be used to calculate the "one turn MAP", used to compute for example the tune. Thus it should not be used for tracking calculations, [13]. A kick code representation of the dipole is possible but becomes very elaborate: The dipole can be replaced by drift-kick-drift combination where the kick describes the focusing effect of the dipole which has to be taken into account for small lattices. A dipole generates however dispersion because of the momentum dependent deflection. The separation of the closed orbits for the different momenta is neglected in this case. Consequently the coordinate system of each particle will be fixed to the specific closed orbit and as a result the particle coordinates are showing only the deviation from the closed orbits. This is in fact no problem if one is interested in the particle position in areas where dispersion is zero. In our case the target will be placed in a dispersive area and the x offset of the particle, measured against the reference orbit, is needed. Thus this method is not applicable. To solve the problem one could try to introduce an additional kick which is creating a dispersion and another one which is destroying it. Nevertheless it is questionable if a model like this could be easily implemented.

Another possibility would be to do separation of the closed orbits in front of the target with a known value of the dispersion (in this case D can be provided by MAD-X). After the target the orbits can be joined together by removing the previously added dispersion shift. In this case the excitation of the horizontal motion can not be studied because the energy loss dependent shift of the closed orbits and the change in the particle oscillation amplitude has to be implemented accurately. Thus this is not a useful alternative.

It is questionable whether symplecticity is needed in our case because the interaction in the target is non-conservative, anyhow. As a first approximation a non-symplectic matrix is implemented, which is generating dispersion.

$$M_{Dipole} = \begin{pmatrix} \cos(\phi) & \rho\sin(\phi) & 0 & 0 & \rho(1-\sin(\phi)) & 0 \\ -\frac{1}{\rho}\sin(\phi) & \cos(\phi) & 0 & 0 & \sin(\phi) & 0 \\ 0 & 0 & 1 & l & 0 & 0 \\ 0 & 0 & 0 & 1 & 0 & 0 \\ 0 & 0 & 0 & 0 & 1 & 0 \\ 0 & 0 & 0 & 0 & 0 & 1 \end{pmatrix}$$

$$\phi = \frac{l}{\rho}$$

ϕ is the bending angle, ρ the bending radius and l the arc length of a dipole sector magnet, [4]. ρ is like k for the quadrupole a function of the momentum and is for each particle recalculated:

$$\rho = \left(1 + \frac{\Delta p}{p_0}\right) \cdot \rho_0$$

The positions x and y and directions x' and y' are computed directly with the transport matrix. The momentum and time delay are not changed by the transport matrix. To estimate the time delay two different methods are taken into account:
First the time delay due to the oscillation around the closed orbit is taken into account by replacing the dipole with the above mentioned kick model. This model is only used for the time estimation. Second the circumference C_0 of the ring is a function of the momentum because of the dispersion. This change can be expressed with the momentum compaction factor α_c which MAD-X, a lattice design program, computes directly:

$$\frac{\Delta C}{C_0} = \alpha_c \cdot \frac{\Delta p}{p_0}$$

The change in circumference leads to an additional time delay. This delay is not calculated in the dipoles, it is calculated in the lattice element where $\Delta p/p$ is changing namely the cavity and the target.

Cavity: The cavity is described with a simple kick. It has a length of zero and does not change the position of the particle but its direction. The cavity changes the energy of the particle by a value δE (see section 1.4.1):

$$\begin{aligned} \delta E &= q \cdot \hat{V} \cdot \sin(\phi_s + 2\pi f_s \Delta t) \\ \delta x' &= -x' \cdot \frac{\delta p}{p} \\ \delta y' &= -y' \cdot \frac{\delta p}{p} \end{aligned}$$

Here $\hat{V}$ is the peak voltage of the cavity, q the charge of the particle, ϕ_s the synchronous phase and f_s the revolution frequency. δp is the longitudinal momentum change which corresponds to the energy change δE. This momentum change δp introduces a small change $\delta x'$ and $\delta y'$ in the direction because the transversal momentum does not change. New values of $\Delta p/p$, x' and y' are calculated after the cavity by adding the small corrections.

Target: The class encapsulates the Geant4 simulation. All new particle coordinates are directly calculated with Geant4. No transport matrix is used in this case. The Geant4 simulation contains the gas wedge target as described in section 3.3 with a target thickness of $0.28\,mg/cm^2$ and a corresponding energy loss of around 300 keV for a 25 MeV particle.

Emittance calculations To study the behaviour of a particle beam in a lattice there is a need to calculate the beam sizes in the different directions namely the emittances in x, y and longitudinal direction. The emittances are computed according to [4]:

$$\begin{aligned} \epsilon_x &= 4\sqrt{\overline{x^2} \cdot \overline{x'^2} - \left(\overline{xx'}\right)^2} \\ \epsilon_y &= 4\sqrt{\overline{y^2} \cdot \overline{y'^2} - \left(\overline{yy'}\right)^2} \\ \epsilon_p &= 4\sqrt{\overline{(\Delta E)^2} \cdot \overline{(\Delta\phi)^2} - \left(\overline{\Delta E \cdot \Delta\phi}\right)^2} \\ \text{whereby} \quad \Delta\phi &= 2\pi f_s \cdot \Delta t \\ \Delta E &= \beta_r \cdot \frac{\Delta p}{p} \cdot p \end{aligned}$$

β_r is the relativistic β, f_s the synchronous frequency and the overlined variables are averaged over all particles.

These emittance calculations are implemented in one special class, so the user is able to place an emittance printout point into the lattice. In our case these emittance printout points are placed in an area where the dispersion is zero. Therefore the closed orbits are not separated and the ellipses in the $x - x'$ phase space have the same centre. The definition of the longitudinal emittance does not include bucket sizes and is therefore simpler, but should also provide the possibility to study the principle behaviour of the production ring.

4.2.3 The lattice

Figure 4.6 shows the resulting lattice of [3]. The parameters can be found in [3]. This lattice is used for the following simulations.

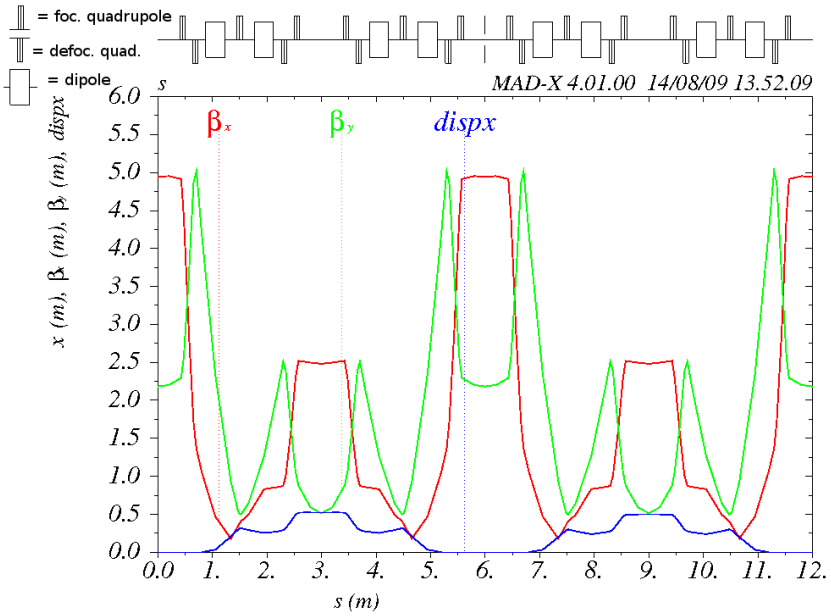

Figure 4.6: The β and D_x function for the lattice used (designed by [3]). On top of it the lattice structure or the ring.

The target is located at $s = 3$, and the cavity at $s = 6\,\mathrm{m}$. The energy loss in the target will be around 300 keV for the reference particle. The peak voltage of the cavity is chosen to 300 kV with a synchronous phase of about 0.34 rad to obtain a energy recovery of 300 keV (the charge of the particles is $+3e$). For simulations without target the synchronous phase is set to zero for longitudinal phase focusing. The emittance printout point is set to $s = 0\,\mathrm{m}$. The dispersion is zero at this point.

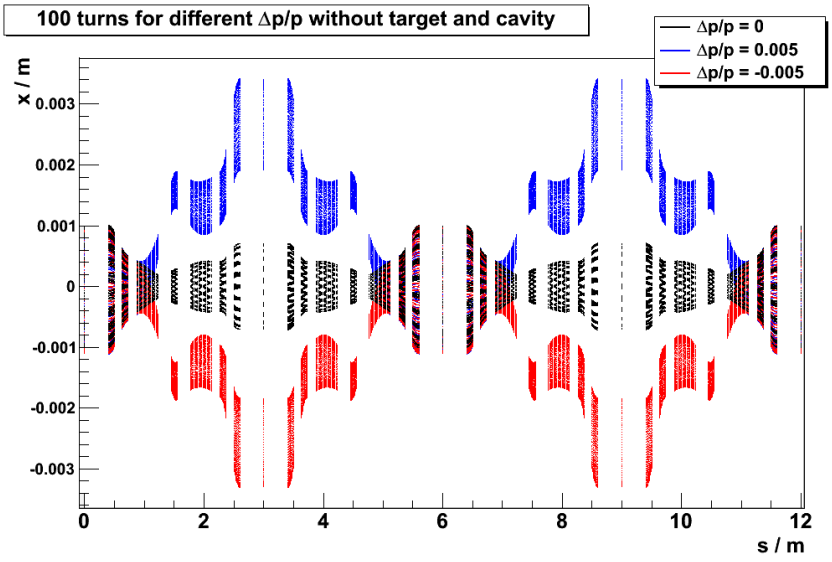

(a) x as a function of s

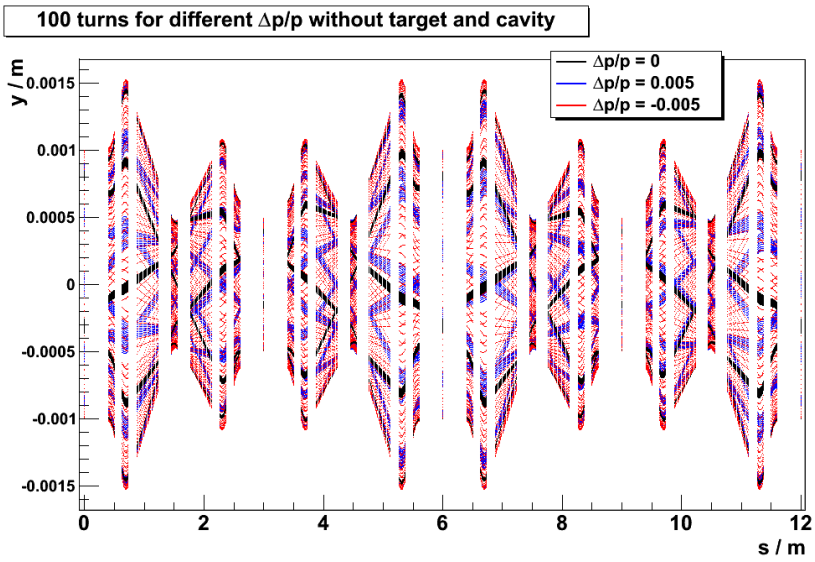

(b) y as a function of s

Figure 4.7: x and y for 100 turns for one particle and different $\Delta p/p$ (red: $\Delta p/p = -0.005$, black: $\Delta p/p = 0$ and blue: $\Delta p/p = 0.005$).

MAD-X calculates the quadrupole strengths to obtain a stable solution for a 25 MeV Li-7 beam. The new tracking code has some limitations in accuracy due to the approximations made. To improve the tracking results the lattice elements are separated into several slices to decrease the step size. The 10 cm long quadrupole are separated into ten quadrupole slices and the 35 cm long dipoles into 20 slices.

Figure 4.7 shows the results of the tracking code for one particle starting with the same position and direction, but different values for $\Delta p/p$. 100 turns are plotted without cavity and target.

On top the x position of the particle is shown as a function of s, the position in the ring. The envelope of black points ($\Delta p/p = 0$) shows the shape of the β-function (more accurately the square root of it), shown in figure 4.6. The red ($\Delta p/p = -0.005$) and blue ($\Delta p/p = 0.005$) points instead show a superposition of the β-oscillation and the separation of the dispersion orbits. The dispersion has at the point of the target a value of $D_x = 52$ cm. With an $\Delta p/p = 0.005$ the shift of the orbits due to the dispersion should be around 2.6 mm. Figure 4.7 confirms the expectation.

At the bottom of figure 4.7 the y position as a function of s is shown. In this case the separation of the different $\Delta p/p$ orbits is not visible because D_y, the dispersion in y direction, is zero in the whole lattice. Something else can however be seen in this picture. The tune Q_y of the lattice must be near a resonance. The black points for the 100 turns of the $\Delta p/p = 0$ particle are accumulated into a few lines. The tracks of the particle seems to reproduce itself after a few turns. The same can be seen for the blue particle. In this case the effect seems not to be so strong as for the black one. The tune Q_y is a function of the momentum and for a certain $\Delta p/p$, Q_y can hit a resonance line in the working diagram. The red particle instead does not show this resonant behaviour. Q_y is probably further away from the resonance.

4.2.4 Comparison with PTC

The new tracking code is tested against PTC which is based on accurate 6-d tracking with Lie transformations [13]. Particles with the same initial conditions are tracked with both codes. The cavity is

included into the lattice to see, if longitudinal phase focusing is working and how accurate the time estimation process is working.

Figures 4.8 show the results of the tracking programs. As starting condition for these simulations the following values are chosen:

$$\vec{z} = (x, x', y, y', \Delta p/p, \Delta t) = (1\,mm, -0.5\,mrad, -1\,mm, 2\,mrad, 0.005, 0\,s)$$

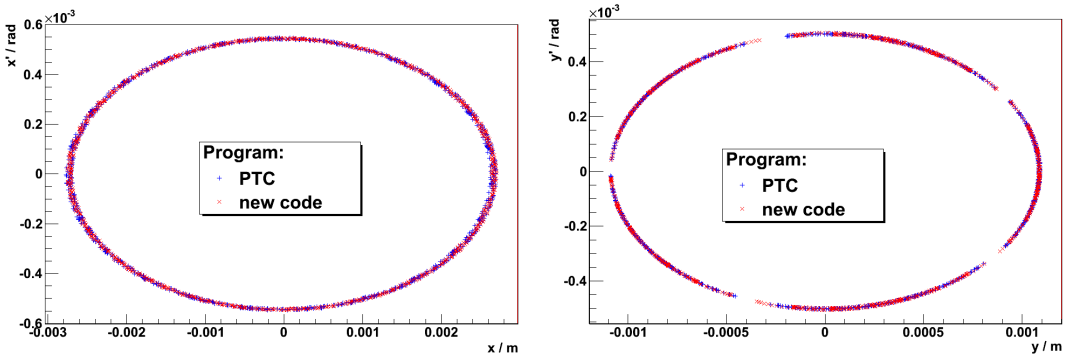

(a) $x - x'$ plane (horizontal phase space)

(b) $y - y'$ plane (vertical phase space)

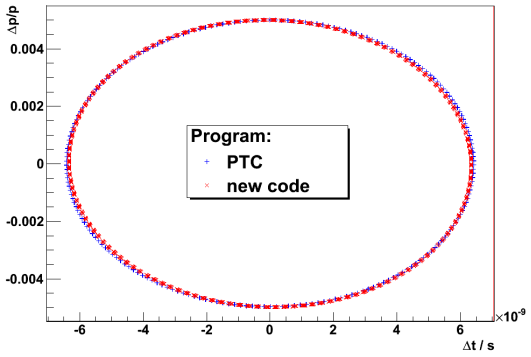

(c) $\Delta t - \frac{\Delta p}{p}$ plane (longitudinal phase space)

Figure 4.8: Comparison between the self-written tracking code and PTC for the same lattice and starting conditions.

The coordinates of the particle are determined each turn at the same position in the lattice namely $s = 0\,\text{m}$, the starting point of the lattice. 1000 turns are simulated and the position of the particle is plotted in the three different phase space planes.

The data points in the different phase space planes almost fall on the same ellipse. The deviations are very small. Only in the $\Delta t - \Delta p/p$ plane, the new tracking code produces a slightly tilted ellipse. All deviations are negligible in size. The only difference between the codes are the position of the calculated data points. This position is directly correlated to the tune. The tune, the programs are producing, are not completely the same. By looking at the $y - y'$ plane, it becomes obvious that Q_y is not far from a resonance, as mentioned above, and both programs show this result. Therefore the difference between the tracking code seems to be small, but visible.

The good accuracy gives confidence in the new tracking code and the code will be used to study

the behaviour of particles in a lattice with a gas wedge target. The purpose of this new tracking code is not to replace an existing and well working code, only a proof-of-concept should be given at the end of the simulations. No coupling between the different planes will be introduced to compensate the heating and damping problem and therefore it will only be possible to track a few hundred turns, but not thousands, until the beam gets unstable. Therefore the lag in accuracy should be tolerable at this stage.

4.2.5 Tracking with target

As a next step the target is included into the lattice. The synchronous phase of the cavity is switched to 0.34 rad. The wedge angle is set to 30°.

To illustrate the tracking, a test particle is started and tracked for several turns. The initial conditions are set to zero in each dimension. This means that the test particle is starting as an ideal particle. Figure 4.9 shows the results for Δt and $\Delta p/p$ as a function of s for ten turns.

As expected the particle reaches the target at $s = 3\,\mathrm{m}$ and looses about 300 keV of energy which corresponds to a change in $\Delta p/p$ of about $6 \cdot 10^{-3}$. The particle reaches the cavity at $s = 6\,\mathrm{m}$ and gains nearly the amount of energy the particle has lost before. Consequently $\Delta p/p$ jumps back to the original level. Because the energy loss is a statistical process, the value of $\Delta p/p$ does not return to the same value. A statistical spread is observed.

Also the time coordinate proofs the expectation. The starting particle is synchronous. Therefore Δt is zero until the particle is arriving at the target. It looses energy and therefore the velocity of the particle is decreased. Consequently Δt is growing because it is measured against a synchronous particle which will not loose any energy. At the cavity the energy is recovered and the velocity of the particle should be again nearly at the same level as before the target. The simulation confirms this expectation: Δt is not growing anymore that strong. The time is increasing for several turns until the time growth is compensated and starts to fall. This behaviour is expected and expresses the phase oscillation of the particle. The particle is oscillating in the longitudinal phase space and the projection on the Δt axis is consequently showing the oscillation which is seen in figure 4.9.

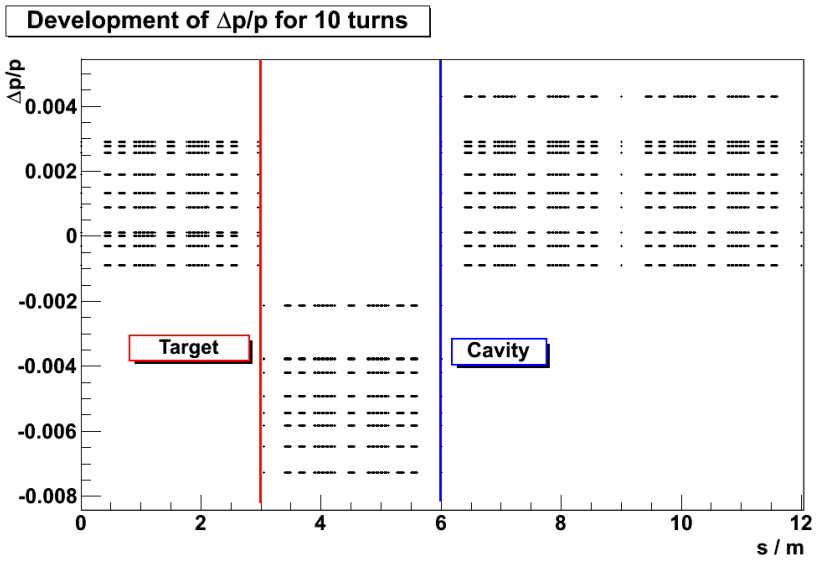

(a) Development of $\Delta p/p$ for 10 turns

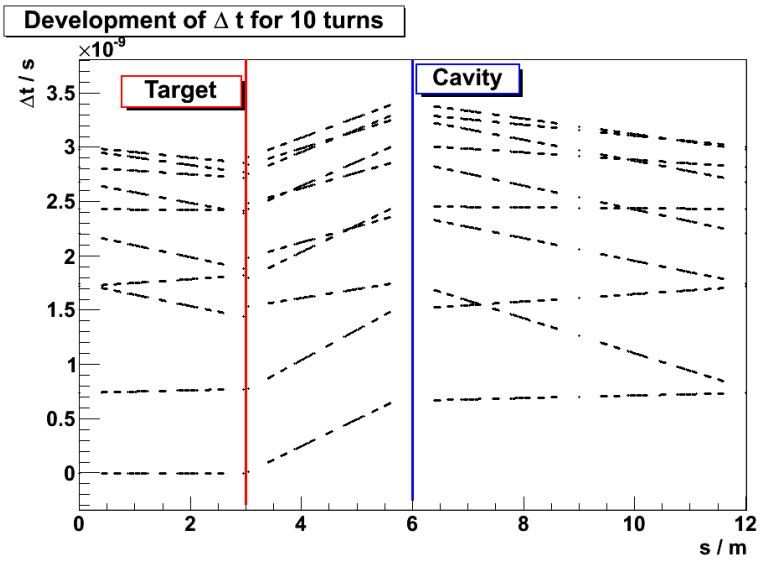

(b) Development of Δt for 10 turns

Figure 4.9: $\Delta p/p$ and Δt as a function of s with target and cavity. The general behaviour is reasonable and confirms the expectation.

The tracking code is working and produces understandable and reasonable results. For the next step not only one particle is tracked, 500 are taken into account to calculate the statistical emittances. It should be possible the see the effects of cooling and heating in the different planes.

For these simulations the lattice with cavity and target is used. Two different wedge angles are choosen, 30° providing longitudinal damping and 1° for heating. The dispersion at the wedge is still 52 cm and the target thickness for the synchronous particle is set to 280 $\mu g/cm^2$.

The 500 particles are statistically distributed in the 6-d phase space. For each dimension a gaussian distribution is assumed with a mean value of zero and a RMS which are calculated from the initial emittance, [4]:

$$\epsilon_x = 2\sigma_x \cdot 2\sigma_{x'}$$
$$\epsilon_y = 2\sigma_y \cdot 2\sigma_{y'}$$

For the longitudinal emittance σ_t (the RMS of the gaussian distribution) is set to 5 ns and $\sigma_{\Delta p/p}$ to 0.01. For ϵ_x a value of 10^{-6} m rad for 30° wedge angle and 10^{-4}m rad for 1° is chosen and for ϵ_y a value of 10^{-4}m rad is set for both angles.

Figure 4.10 shows the results of the simulations. Only around 100 turns can be studied until the emittances show the expected instabilities. Also the target has geometrical limitations. If the emittances in x or y become to large, the particles start to miss the target or leave the world volume of the Geant4 simulation too early which affects for example the time estimations. In those cases the results are not representative anymore. In the simulations below this problem does not occur in the first 100 turns. The quadrupole strengths are not optimized to get tunes far away from resonances. This leads to special artefacts in the y phase space.

The plots at the top of 4.10 show the longitudinal emittance as a function of turns. As expected for the small angle ϵ_p is growing exponentially. The angle and therefore $V = D_x \cdot \partial U/\partial x$ is not large

enough to swap sign in the longitudinal damping rate. This is the case for 30° wedge angle and therefore longitudinal cooling take place.

The opposite effect should take place in the horizontal plane. A heating is expected for a wedge angle which is too large and indeed this can be seen in the simulation for 30° wedge angle. Consequently a cooling should be seen for 1°. The emittance is growing on the first turns and is nearly stabilised for the rest of the 100 turns. ϵ_x is however still slightly growing. One have to take also other effects like the scattering in the target into account. This processes compensates the cooling of the emittance and leads to a stable emittance. If the 500 particles start with an emittance below this point, the emittance will approach from the bottom to this stability region. This could be the case in the simulation above. There is no strong heating which leads to an uncontrollable behaviour in the horizontal plane.

In the vertical plane one would expect similar behaviour for both wedge angles since the target is translation invariant in y and the dispersion D_y is zero in the whole lattice. The scattering process in the target produces kicks in y' with an RMS of the distribution which is depending on the thickness of the target. The thickness itself is a function of x because of the non-zero $\partial U/\partial x$. This leads to a correlation between x and y, but the effect should be small and not visible by looking at only 100 turns. In fact both simulations produce the same behaviour except for statistical fluctuations. The emittance is shrinking overall after a first strong growth but there are some large drops around turn $20, 40, 60$ and 80. It is interesting to see that at nearly the same turn numbers some large oscillations in the longitudinal emittance are visible. Possibly at these points some resonances are hit which leads to an unexpected behaviour. Moreover the whole lattice is at this point not optimized to get a very good placed tune in the working diagram. By doing this, one could possibly prevent some artefacts which are seen in figure 4.10. The whole production ring simulation is at all very complicated and there are a lot of different settings which can be varied and optimized. For example the phase and the peak voltage of the cavity have a strong influence on the results.

Eventually those optimizations and studies have to be done and also the implementation of the tracking code has to be chross-checked to be sure that everything is running and working fine. Unfortunately this can not be done as part of this thesis. The results only give a first proof-of-concept.

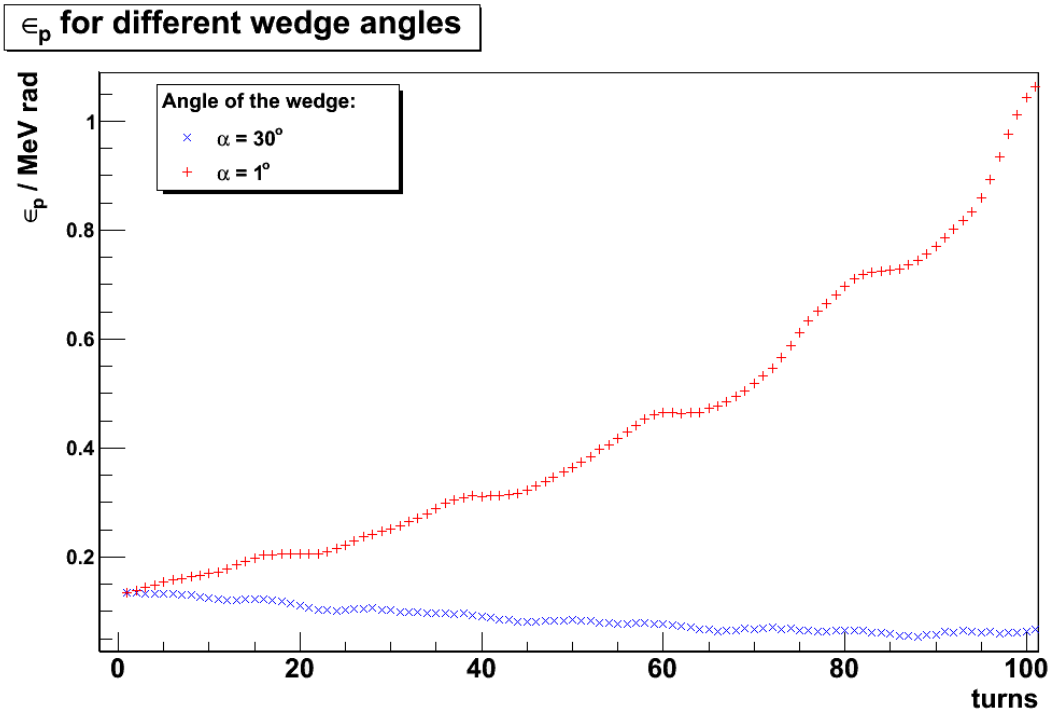

(a) ϵ_p as a function of turns

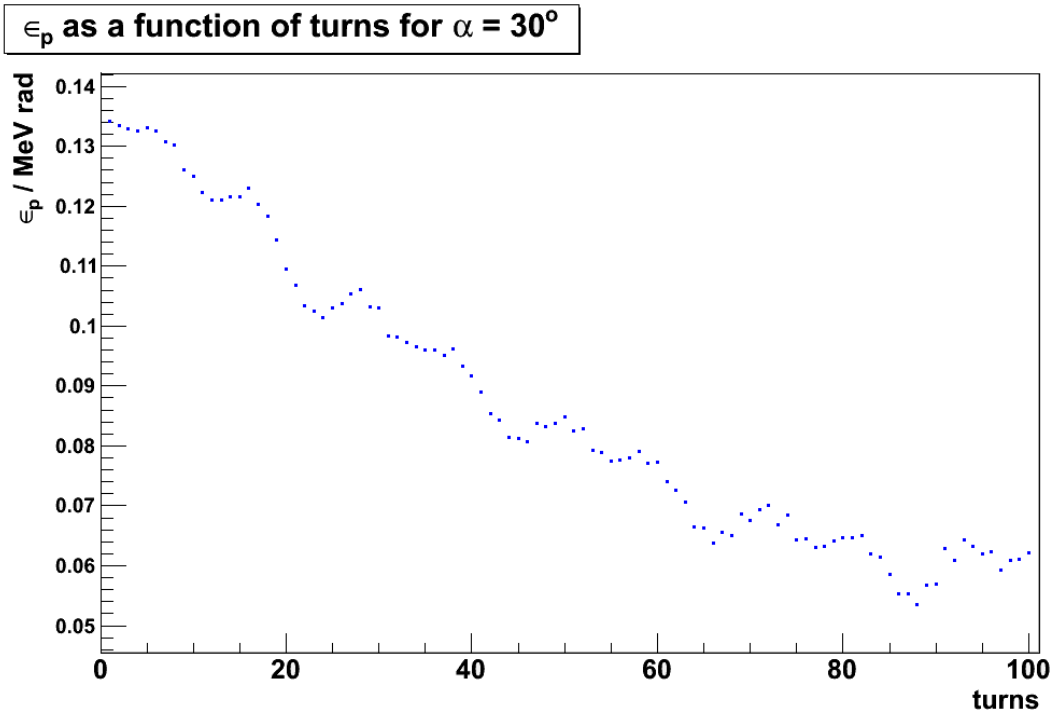

(b) ϵ_p as a function of turns (detailed view for 30° wedge angle)

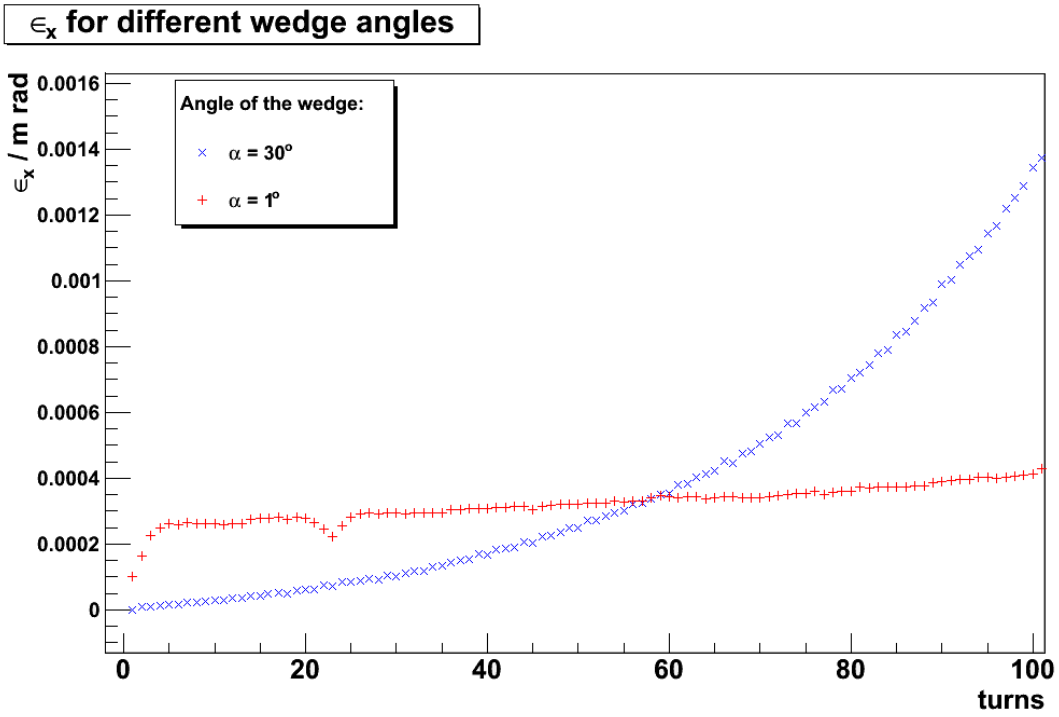

(c) ϵ_x as a function of turns

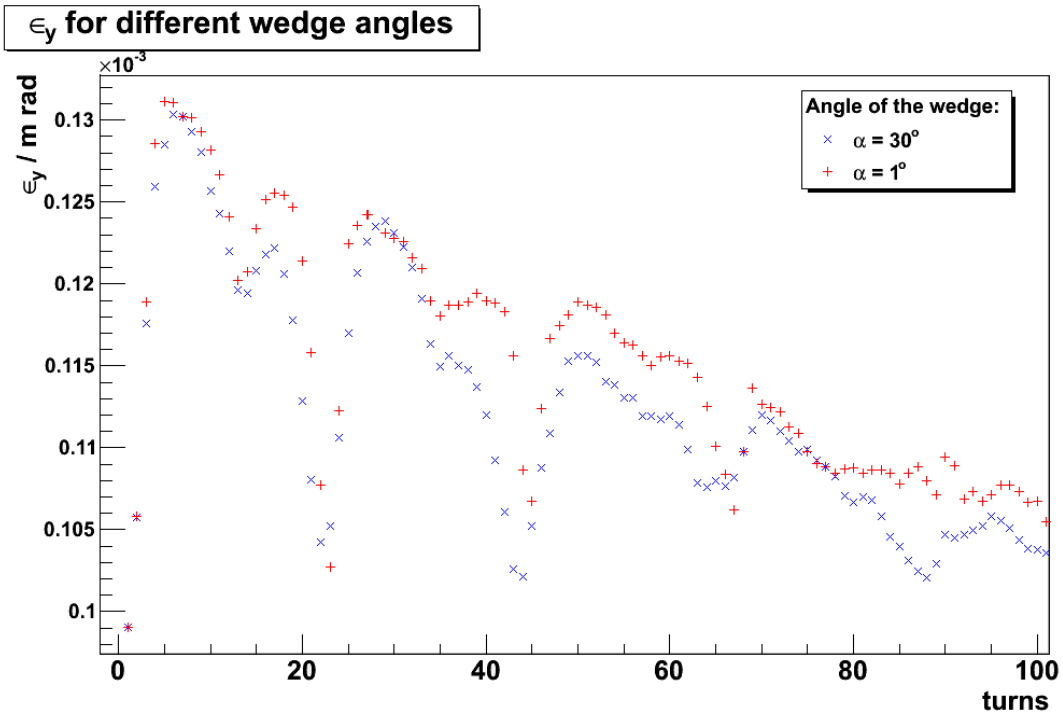

(d) ϵ_y as a function of turns

Figure 4.10: Emittances as function of turns for two different wedge angles (red: 1°; blue: 30°)

5 Conclusion

Hadronic model studies in Geant4

The models for the inelastic hadronic interaction, implemented in Geant4, are studied. Two models, which are able to describe the reactions, are used below the validity range. Thus it is not surprising that the models are not consistent with each other. A comparison of the reaction cross section with measurements have shown that both models are not valid at these energies by using the recommended models for the inelastic cross section. Possibly modifications can be made to trim the models so that they are able to reproduce the measurements. The look at the kinematics have also not shown a consistent image. Which of the model is in this case more accurate can not be answered without measurements. This needs to be done in the future if Geant4 should be used for simulations like that.

Longitudinal cooling

Geant4 is used to transcribe the condition for longitudinal cooling to requirements, the gas wedge and the dispersion of the lattice have to fulfil. Thus a lattice can be designed which provides a sufficient large dispersion. This is necessary to swap sign in the longitudinal damping rate by increasing J_ϵ. The corresponding decrease of the partition number J_x has to be counterbalanced between J_x and J_y by introducing coupling between the horizontal and vertical motion of the particles. The condition for $J_\epsilon = 0.13$, as suggested by [2], is derived. The results of the simulations have to be checked via tracking simulations and to study the heating and cooling concept.

Tracking

Representative model: Assuming Geant4 is accurate at the studied scenarios and beam energies, the parameters of scattering distribution are studied and determined. A well-known formula, describing the RMS scattering angle, is used outside the validity range and therefore corrected by a fit for this purpose to reproduce the scattering results of Geant4. The energy deposition is compared with the Bethe-Bloch formula. The deviations between the unintegrated formula and the via Geant4 simulations calculated energy losses are small for energies above 10 MeV. The RMS of the energy loss distribution is determined. With these parameters an implementation of a kick based representative model by using random number generators is possible. This implementation is done by [3] and included in a 6-d phase space tracking code called SixTrack.

Tracking code: As part of this thesis, another way is taken to study the behaviour of the whole production ring: A new tracking code is written in C++ in a Geant4 like style. Thus a combination of target simulation within Geant4 and tracking simulation can be done easily. Due to the small time frame, available for the implementation, strong assumptions and approximations are made. Nevertheless the accuracy of the tracking program is good enough for those kind of simulations at a first view, but needs to checked in the future. Studies with the implemented representative model in SixTrack will show whether the implemented tracking code or the representative model is accurate enough to study the production ring behaviour. First studies with the new code and target implementation have shown that the program is delivering understandable results but also that the whole project is complicated. A proof-of-concept of the heating and cooling behaviour of the production is given. The lattice needs to optimized to avoid artefacts which probably are caused by a wrong placed tune in the working diagram. There is a lot of work to do in the future to study the ionization cooling process in detail. Finally

additional coupling between the different phase space planes needs to be introduced to achieve and to study in each direction a cooling effect.

Bibliography

[1] C. Rubbia, A. Ferrari, Y. Kadi, and V. Vlachoudis. Beam cooling with ionisation losses. *Nucl. Instrum. Meth.*, A568:475–487, 2006.

[2] David Neuffer. Low-energy ionization cooling of ions for beta beam sources. *Nucl. Instrum. Meth.*, A585:109–116, 2008.

[3] Michaela Schaumann. Development and lattice design of an ion production ring for a beta beam neutrino facility.

[4] CERN. *CAS - CERN Accelerator School : 5th General Accelerator Physics Course*, September 1992. Jyväskylä, Finland.

[5] Dr. Gunter Folger. Private communication.

[6] *Geant4 physics reference manual*, December 2008. Online available on http://geant4.cern.ch.

[7] K. Niita et al. Analysis of the (N, x N-prime) reactions by quantum molecular dynamics plus statistical decay model. *Phys. Rev.*, C52:2620–2635, 1995.

[8] *Geant4 User's Guide for Application Developers*, June 2009. Online available on http://geant4.cern.ch.

[9] Harald Enge. *Introduction to nuclear physics.*

[10] S. N. Abramovich, B. JA. Guzhovskij, A. G. Zvenigorodskij, S. V. Trusillo, and S. A. Dunaeva. The investigation of the 9Be high excited states in the 6Li(t,p)8Li and 7Li(d,p)8Li reactions.

[11] J. P. Schiffer, G. C. Morrison, R. H. Siemssen, and B. Zeidman. Study of the (d, p) Reaction in the 1p Shell. *Physical Review*, 164:1274–1284, 1967.

[12] Particle Data Group. Particle physics booklet, July 2008.

[13] Dr. Werner Herr. Private communication.

[14] Dr. Bernhard Holzer. Private communication.

Erklärung

Hiermit versichere ich, dass ich die vorliegende Arbeit selbstständig verfasst und keine anderen als die angegebenen Quellen und Hilfsmittel benutzt sowie Zitate kenntlich gemacht habe. Die Arbeit ist in gleicher oder ähnlicher Form noch nicht als Prüfungsarbeit eingereicht worden.

Aachen, den